Building and Environment 210 (2022) 108700

Contents lists available at ScienceDirect

Building and Environment

journal homepage: www.elsevier.com/locate/buildenv

Laboratory testbed and methods for flexible characterization of thermal and fluid dynamic behaviour of double skin facades

Aleksandar Jankovic [a], M. Salman Siddiqui [a,b], Francesco Goia [a,*]

[a] Department of Architecture & Technology, Norwegian University of Science and Technology, NTNU, Trondheim, Norway
[b] Faculty of Science and Technology, Norwegian University of Life Sciences, NMBU, Ås, Norway

ARTICLE INFO

Keywords:
Double-skin façade
Experiment
Climate simulator
Design of experiments
Airflow
Taguchi design
Velocity profile method

ABSTRACT

Heat and mass transport in double skin façades (DSFs) are complex phenomena driven by boundary conditions and are in constant non-linear interaction with the constructional elements of the DSF. Comprehensive experimental investigations to understand these complex behaviors are usually rigid, time-consuming and expensive. In this paper, we present the concept and the features of a flexible experimental testbed that, in conjunction with optimized experimental procedures, can facilitate comprehensive investigations and performance assessment of DSFs. The testbed, which consists of an adjustable DSF mock-up placed into a climate simulator, allows many DSF configurations to be investigated in combination with a wide range of boundary conditions. Several methods for different types of experimental investigations with various levels of complexity are presented: standard metrics measurements, one-factor analysis, design of experiments and dynamic profile measurements. By providing examples and discussing the limitations, challenges and possibilities of each investigation method, the paper aims to provide an overview of different characterizations suitable to assess how different constructional features and boundary conditions affect the performance of DSFs. Experimental data collected during this study are also made available in a data repository for future independent scientific analyses of DSF thermophysical behavior or numerical models' validation.

1. Introduction

A double-skin facade (DSF) is a building envelope system that consists of an internal and external layer, usually highly transparent, with a cavity between the two skins, which is ventilated with air, and where a device for a solar and visual gain control can be installed [1]. This building envelope technology originates from the need to assure high occupant comfort [2] and effective heating, cooling, indoor air quality and daylighting control strategies [3] in the context of highly transparent building envelopes. Due to greater complexity than standard, single-skin envelope elements, finding the optimal configuration (both in terms of construction features and operational modes) for a DSF that assures the best performance across multiple domains is often rather challenging [4]. Physical processes, including transport of mass, momentum and heat/energy, are driven by the surrounding environment and are affected by the constructional features. Therefore, they are more challenging to predict in a DSF than in a single-skin facade [5], and this complexity directly impacts the reliability of the design solutions adopted for DSFs.

The complex interrelation of physical processes occurring in a DSF system can be investigated through experimental studies, thereby expanding our understanding of how constructional features and operational modes can be fine-tuned to achieve a given performance. In addition to this direct knowledge gain, experimental characterizations represent a source of data to validate numerical models. Systematic experimental investigations and robust validations of numerical models can only be achieved if a sufficiently large range of possibilities is experimentally tested in terms of boundary conditions, construction features and operational modes – something that is difficult to achieve by testing one particular DSF configuration in a specific building or testing condition.

Many experiments have been performed so far with different levels of complexity, of which the largest number makes use of outdoor natural boundary conditions [6–23]. The major limitation of this type of experiment is that they do not allow one to set specific boundary conditions deliberately, and to isolate certain effects to focus the study on one or more particular aspects is also quite challenging in most cases. Experiments in a controlled environment can instead offer conditions that overcome these limitations and thus represent a powerful tool to

* Corresponding author.
E-mail address: francesco.goia@ntnu.no (F. Goia).

https://doi.org/10.1016/j.buildenv.2021.108700
Received 30 September 2021; Received in revised form 26 November 2021; Accepted 19 December 2021
Available online 22 December 2021

Nomenclature

Symbols

C	Thermal conductance [$Wm^{-2}K^{-1}$]
c	Specific heat capacity [Jkg^{-1} $^oC^{-1}$]
co	Contribution [%]
d	Depth [cm]
err	Error [depend on the quantity]
g	Solar factor, g-value [−]
h	Surface heat transfer coefficients [$Wm^{-2}K^{-1}$]
I	Solar irradiance [Wm^{-2}]
$\dot{m}$	Air mass flow rate [kgs^{-1}]
q	Heat flux density, heat flux rate [Wm^{-2}]
p	p-value [−]
t	Temperature [^oC]
U	Thermal transmittance, U-vlaue [$Wm^{-2}K^{-1}$]
V	Airflow rate [m^3h^{-1}]
Δ	Difference [−]
φ	Angle [°]
γ	Dynamic insulation efficiency [−]
τ	Direct solar transmittance [−]

Subscripts

cav	refer to cavity
e	refer to efficiency
HFM	refer to heat flux meter
i	refer to inner
ic	refer to the inner half-cavity
ig	refer to the inner glazing
ii	refer to the inner side of inner glazing
in	refer to the incident
io	refer to the outer side of inner glazing
net	refer to net gain/loss
o	refer to outside
oc	refer to the outer half-cavity
oi	refer to the inner side of outer glazing
og	refer to the outer glazing
oo	refer to the outer side of outer glazing
p	refer to constant pressure
sh	shading
tr	refer to transmitted
vent	refer to convective heat gain/loss that is absorbed/released by the airflow that passes through the cavity

Acronyms

AM	Ante meridiem, before noon
ANOVA	Analysis of variance
ADC	Analog-to-digital converter
BIG	Big size of the opening
CO2	Carbon-dioxide
D	Depth
DOE	Design of experiments
DSF	Double skin facade
I–I	Indoor air curtain
ISO	International standard organization
ISR	Solar irradiance
F	Factor
FPGA	Field Programmable Gate Arrays
H	Height
HFM	Heat flow meter
L	Level
MED	Medium size of the opening
O–O	Outdoor air curtain
PIV	Particle image velocimetry
RH	Relative humidity of air
RTU	Remote terminal unit
SHGC	Solar heat gain coefficient
SHTC	Surface heat transfer coefficient
SMALL	Small size of the opening
SMI	Standard motor interface
T	Air temperature
TD	Taguchi design
VB	Venetian blinds
VPM	Velocity profile method
W	Width

systematically assess, both in-depth and in breadth, the thermo-physical behavior of DSF systems. Equipment for controlled experiments usually only allows one to perform tests in steady-state conditions, where a particular performance indicator is examined in response to a combination of controllable factors maintained at constant levels. Traditionally, due to the historical focus placed on the performance in relation to a certain thermal gradient, the majority of these experiments were performed in conditions where only the thermal environment was included in the characterization, and analyses of DSF systems have followed this trend too [24–31]. Experiments where both thermal gradient and impinging radiation (to replicate the effect of solar radiation) are controlled are much rarer [32–34] due to an increase in the complexity of the equipment required to carry out these tests. There is no evidence in the literature of experiments where all the flow drivers (incident solar radiation, temperature, and wind) are controlled simultaneously.

To increase the possibilities for systematic performance characterization and theoretical investigation of DSF systems, we have developed, in the framework of a dedicated research project [35], a flexible testbed that gives researchers an extensive range of possibilities to fill the existing knowledge gaps and provide the research community with a comprehensive experimental dataset for model validation. The testbed we have conceived is made of an adaptable DSF mock-up installed into a state-of-the-art climate simulator equipped with integrated artificial sun lamps. The features of our characterization system make it possible and (relatively) easy to investigate an extensive range of DSF configurations, operational modes and boundary conditions, making it possible to deepen the knowledge of how constructional features and operations, environmental factors and their interactions influence the thermal and fluid dynamics behavior of DSF systems.

The aim of this paper is to present the concept, design and features of the experimental set-up, to report its verification and calibration, and to demonstrate, through a series of exemplification studies, the possible investigation methods that can be adopted to address open questions about the thermal and fluid dynamics behavior of DSF facades. The array of experimental methods shown in this article aims to highlight how different methods, rather than being alternative techniques to study the same aspect, are complementary approaches that target the many ways of studying and assessing the behavior of a double skin façade. Through this, we aim to illustrate how different performance metrics that address different phenomena are necessary when studying the performance of DSFs.

In an effort to enable the whole scientific community to access experimental data for further analysis or for model validation purposes, we release together with this paper a set of experimental data collected during the first tests carried out with the use of the newly developed testbed. In this context, the paper also becomes an essential tool for understanding how to read and understand publicly released experimental data.

The remainder of this paper is structured as follows. In Section 2, we present the experimental set-up, with the characteristics of the flexible mock-up, the experimental facility, hardware and software for controlling and monitoring the experiment. In Section 3, we focus on the different methods that can be employed in combination with the flexible testbed. We report therein the details about the verification and calibration of the experimental set-up, and then present four methods for the characterization of thermal and fluid-dynamics behavior of DSF, namely a method for standardized metrics measurements, the one-factor analysis, the design of the experiments (DOE) and dynamic profile measurements. In Section 4, we demonstrate the use of the testbed and the different methods by showing the results of four investigations. Though the focus of the paper is not placed on the results obtained through the different experimental runs, we briefly discuss in this section the significance of some of the findings. In Section 5, we discuss the challenges and limitations of the different experimental investigations carried out with the newly developed testbed. We also reflect on the possibilities enabled by this experimental system and on how different methods and investigations can target different ways of assessing the behavior of DSFs.

2. Experimental testbed

2.1. The flexible DSF mock-up

A new flexible testbed has been realized and designed to operate in combination with the climate simulator so the current knowledge on the thermal and fluid mechanical behavior of DSF can be expanded [3]. A mock-up is equipped with a sequence of different actuators allowing, in combination with a climate simulator, a systematic and parametric analysis of the performance of tested DSF technology [4]. Different cavity depths ranging from 200 to 600 mm, the angle and the presence of venetian blinds and the airflow produced by the fans can be manipulated systematically. Furthermore, it is possible to control the airflow path by opening and closing the corresponding vents on the tested element. In combination with a climate simulator, a testbed offers high flexibility in testing desirable configurations and boundary conditions, both in a steady and transient state. The physical properties of DSF are monitored through more than seventy sensors for the acquisition of temperature, airflow, relative humidity, differential pressure, irradiance and many more.

2.1.1. DSF mock-up specifications

Test-sample is a full-scale DSF consisting of inner and outer transparent skins mounted into the aluminum frame with a thermal break (Fig. 1a). Both skins are composed of 4 mm thick double glazing with a 15 mm gap filled with a mixture of air and argon (1–9 ratio). The outer pane is clear, while the inner pane is low-E glass with a coating applied on the side in contact with the gap. The glazing area is 3.92 m^2 (W - 1.4 m X H – 2.8 m). Space between the inner and outer skin can be ventilated and contains venetian blinds as a shading device. It is possible to change its depth between 20 and 60 cm thanks to a scissor system driven by the unidirectional electrical motor (24V). The shading device is equipped with 58 slats painted in white aluminum color (RAL 9006) with estimated reflectivity between 0.5 and 0.6, length of 150 cm and width of 5 cm. Venetian blinds can be lowered and raised, and the angle of slats can be adjusted between 90^0 and near to 0^0 (closed). The DSF has four openings, two placed in the outer skin (one at the bottom and one at the top) and two placed in the inner skin (again, at the bottom and at the top). This feature makes it possible to obtain different airflow paths depending on which two of the four possible openings are kept open. Closing all four openings means maintaining the DSF in the thermal buffer state, thus insulating the ventilated cavity from both the outdoor and the indoor environment. In the experimental investigations presented in this paper as a demonstration of the test bed functionality, we have tested three airflow paths: thermal buffer (no airflow path, TB), indoor air curtain (I–I) and outdoor air curtain (O–O) ventilation modes. In the I–I airflow path, the ventilated cavity receives air from the indoor environment (usually through the bottom opening) and releases the air again to the indoor environment (usually through the top opening). In the O–O ventilation mode, outdoor air usually enters the cavity through the lower opening on the outer skin and leaves the cavity through the upper opening on the same side, thus returning to the outside environment (Fig. 1b). The flow inside the cavity can be driven mechanically by ten small fans (SanAce 60L) with dimensions of 60 × 60 × 25 mm^3 installed at the top of the cavity.

2.1.2. Measurement system

In order to obtain the desired information on the thermal and fluid dynamics behavior of DSFs, both thermal and velocity fields were

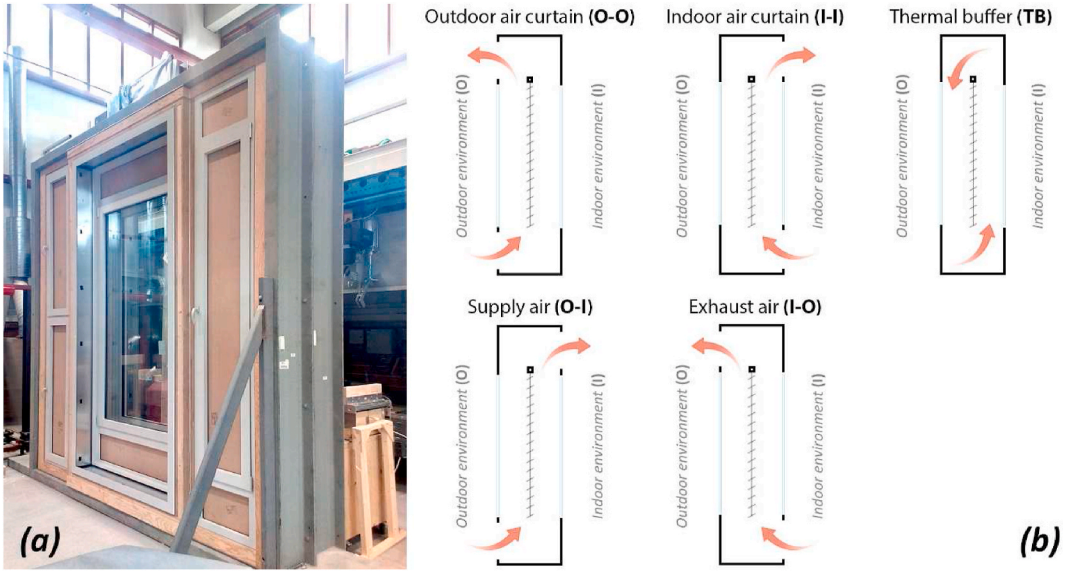

Fig. 1. ***(a)*** The façade mock-up assembled in the metal frame ready for installation in the Climate simulator. At the two sides of the mock-up with an expandible cavity, two cabinets host the monitoring and control system and a ventilation section for airflow calibration. (***b)*** Possible ventilation paths allowed by the façade mock-up.

intended to be monitored in the cavity, as well as the temperature and incident radiation distribution on the glazing surfaces. In addition to these, several other quantities were also recorded, leading to a large number of instruments (more than 70) installed in the test bed, as described in Table 1. Pyranometers were employed to measure incident solar radiation on the outer surface of DSF and the transmitted solar radiation into the indoor room. The air temperature was measured in the indoor and outdoor room at three heights, while in the central height, besides air temperature, relative humidity was measured as well. Hot-wire anemometers were placed in 12 positions along three heights in the cavity so that profiles of the temperature and vertical component of velocity could be obtained (Fig. 3). Near the inlet and the outlet, the air temperature was measured in the four positions, two in the inner and two in the outer part of the cavity. Pressure difference was measured along three paths: across the inlet, across the outlet and along the cavity. Resistance temperature sensors (pt100) were placed at the four glazing surfaces to measure temperature along three heights and additionally temperatures of the frame between the openings and inner-outer and outer-inner glazing. Heat flux density through blinds and four glazing surfaces was measured, where two heat flux plates were connected in the series to determine the average heat flux that passes through inner-inner and outer-outer glazing. An ultrasonic airflow meter was placed in the airflow box to calibrate different techniques to assess airflow rate. Five photovoltaic pyranometers were placed on the outer-outer glazing to evaluate the uniformity of incident solar radiation. We implemented best-practice solutions, as available in the literature [36], to reduce to influence of solar irradiation on the measurements of temperature, heat flux and velocity (the absorption of the incident solar radiation by the sensors' surface may lead to incorrect values). For example, HFMs were protected with adhesive reflective aluminum tape from additional heating by absorbed solar radiation. Protection against irradiance and normal ventilation of the surface temperature sensors was enabled by placing them under a hollow half-cylinder with a highly reflective outer surface. A plate of high reflectivity protected the side of the hot wire-anemometers exposed to the solar simulator (Fig. 2).

2.1.3. Onboard system for monitoring and control

Since many sensors were needed for monitoring, it was almost impossible to manage them manually. Instead, a system for automatic control and monitoring of the experiment was developed. A communication system was developed based on the sensor's output signal (analog voltage or current or digital RS-485). All sensors were connected to the multiplexing station composed of several acquisition cards, and 13 analog-to-digital converters (ADC) were used to combine multiple analog and digital signals into one digital signal. The multiplexing station was connected to the RS-485 port of the microcontroller – Compact Single-Board Controller (National instrument sbRIO: 9627) equipped with Field Programmable Gate Arrays (FPGA), which enabled sbRIO 9627 to work both as the source of the output signal and the receiver of the data from the sensors and ADCs.

Monitoring and data acquisition software deployed on the sbRIO: 9627 was developed in the LabVIEW environment. This platform contains a library of function tools based on which system for monitoring and control is developed. The Modbus library was extensively employed to control 13 ADCs used to collect analog signals from transducers and transmitters and convert them into a Modbus RTU signal. The system for monitoring and control was equipped with a graphic interface and developed to manage the measurements and main features of the test facility (cavity depth, fans rotation, shading proximity to glazing, and blind angle). The sampling data from sensors was set to the interval of 10 s, but various options were enabled to suit the data acquisition frequency for different types of tests, including averaging of values. Most of the sensors and all ADCs used the RS-485 protocol to communicate with the sbRIO 9627.

2.2. Climate simulator

The DSF mock-up was installed into a large metal frame that allowed the sample to be placed in the climate simulator, which is an indoor experimental facility designed to simulate indoor and outdoor conditions in terms of air temperature and humidity, rain, incident solar radiation and pressure difference. The Climate simulator has a total installed power of 40 kW and consists of two test cells; one is intended to simulate the outdoor environment and the other to simulate the indoor environment (Fig. 4a). Both rooms are insulated with 120 mm thick high density (40 kg/m^3) polyurethane foam with thermal conductivity of 0.0265 W/(mK). A test sample needs to be installed in the steel or wooden frame and placed between two rooms (Fig. 4b). Since the dimensions of the test sample can measure up to 3.9 m in height, 3.6 in width and 0.8 in thickness, placing the frame and test sample in the required position is done using a bridge crane. The outdoor room measures 3700 × 1500 × 3240 mm^3 (W x D x H) and has a solar simulator (sun simulation system) and rain test system installed. The air temperature can be simulated in the range between −20 and 80 °C with an accuracy of ±0.3 °C and a maximum rate of 0.5 °C/min. However, some limitations were experienced when particular combinations of temperature and solar irradiation were requested, as further specified further below.

Relative humidity can be replicated in the range of 20–95% without simultaneous use of the solar simulation system and in the range between 20 and 50% otherwise. The rain test system can produce rain intensity in the range of 10–100 dm^3/(m^{2}h) with droplet size between 15 and 35 μm. The indoor room has the same dimensions as the outdoor room and can regulate the temperature, in the range 5 and 50 °C with an accuracy of ±0.3 °C and relative humidity in the range 20 and 95% with a precision of ±3%.

The system simulating solar radiation consists of the array (3 × 3) of metal halide lamps, and it is placed on the special wall construction facility with a surface 2400 × 2400 mm^2. According to technical specifications, irradiation power is 1000 W/m^2 at a 760 mm distance from the light source with a homogeneity ±10%. It must be pointed out here that homogeneity of the incident solar radiation on the tested DSF sample within these limits is sometimes tricky to achieve, primarily due to deteriorating imperfection of the solar simulator and different ages of lamps (hours of usage). Furthermore, it is important to mention that the directionality of the emitted radiation cannot be controlled. The array of 9 lamps, which are evenly distributed in front of the sample area, and each equipped with a reflector that focuses the radiation towards the test zone, can't be oriented. Part of the radiation that leaves the array reaches the test specimen in a relatively narrow range close to the normal angle to the specimen's surface, and another part of the radiation that leaves the array behaves as diffuse radiation, reaching the specimen without a particular direction. This feature limits the capability to study in detail the relation between radiation direction and the DSF's shading device, but still allows one to analyze the role and the impact of the shading device, and even of different degrees of opening of the shading device, in relation to the intensity of the solar radiation.

The metal halide lamps installed in the array were specially designed for accurate sun simulation and continually emitted a spectrum very close to natural sunlight. The intensity of each lamp can be controlled with a resolution of 1% in a range between 50 and 100% of the maximum electric power drawn (2500 W). That may pose a problem if one wants to replicate conditions with low solar radiation, such as winter days or a gradual increase/decrease in incident solar radiation during sunrise/sunset. The default distance between light source housing and the outer surface of the test sample is approximately 1.05 m. In the specific case of the flexible DSF mock-up, where the cavity depth can be changed by retracting the inner or outer skin, it was observed that actual solar irradiance impinging on the façade mock-up depends on the distance between the sample and simulator, and it diminishes when the distance between the façade's outer skin and the lamp's array increases.

Table 1
Characteristics of the sensors used in the experimental campaign.

Sensor type	Manufacturer (model)	Signal	Outside	Bottom openings	Outer-outer	Outer-inner	Outer half-cavity	Shading	Inner half-cavity	Inner-outer	Inner-inner	Top openings	Inside	Airflow box	Quantity	Symbol	Accuracy/ uncertainty (in a considered range)
Pyranometer	DeltaOhm (LPPYRA03ACM12)	4 … 20 mA	1										1		2	1	Second class pyranometer (ISO 9060)
Air temperature and relative humidity sensor	DeltaOhm (HD48S17TV)	Digital (RS485)	1										1		2	2	RH: ±1.5 %RH for (0 … 90 %RH) t: ±0.3 °C for (0 … 70 °C)
Air temperature sensor	DeltaOhm (HD48S07TV)	Digital (RS485)	2										2		4	3	±0.3 °C for (0 … 70 °C)
Hot-wire anemometers	DeltaOhm (HD2937TC1.5)	4 … 20 mA					6		6						12	4	v: ± (0.1 m/s+3% of meas.) for (0 … 1 m/s) and t: ±0.3 °C
Air temperature sensor	DeltaOhm (HD4807TC1.5)	4 … 20 mA					4		4						8	5	±0.3 °C for (0 … 70 °C)
Differential pressure meter	DeltaOhm (HD404T1PDAZ)	4 … 20 mA or 0 … 10V		1			1		(1)			1			3	6	±1.5% of range (± 50 Pa) for (0 … 50 °C)
CO_2 concentration sensor	DeltaOhm (HD37BTC)	0 …. 10V	1												1	7	± (50 ppm +3% of meas.) for (0 … 2000 ppm) at 20 °C, 50 %RH
Airflow sensor	Lindab (Ultralink monitor FTMU)	Digital (RS485)												1	1	8	±5% of meas. or ±2.0 l/s for 200 mm diameter
Resistance temperature detector Pt100	SterlingSensors (Rubber Patch)	3 wire PT100			4	6		4		6	4				24	9	Class B (IEC 60751:2008)
Heat flux plate	Hukseflux (HFP01)	±120 mV			2	2				2	2				8	10	Calibration uncertainty: <3% In ideal conditions: ±6%
Heat flux film	greenTEG AG (gSKIN XM 26 9C)	±600 mV						2							2	11	Calibration uncertainty: ±3%
Photovoltaic pyranometer	Soluzione Solare (LM1-10V PRO)	0 …. 10V			5										5	13	Calibration uncertainity: I: ± 3.5%, t: ±1.5 °C

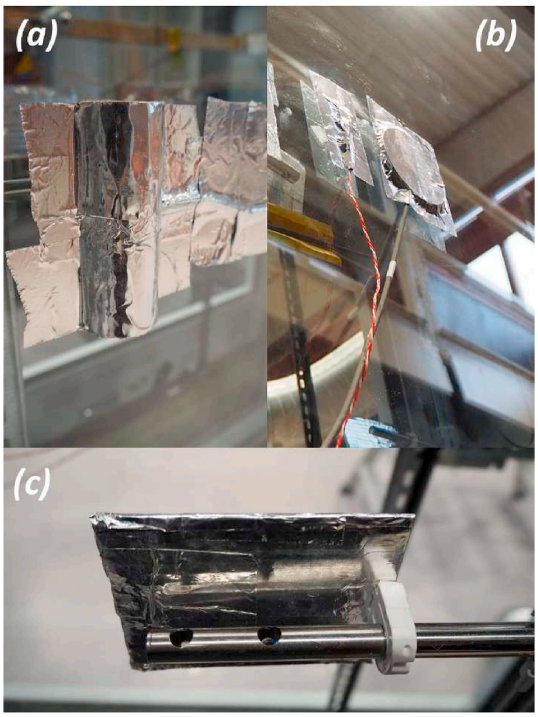

Fig. 2. Shielding of the sensors to avoid influence of solar radiation. (a) Shielding of surface temperature sensors. (b) Shielding of heat flux meters. (c) Shielding of hot-wire anemometers.

Furthermore, accurately maintaining the set-point temperature in the outdoor chamber when the solar simulator is active is not trivial, primarily when a high level of irradiance is used and very low air temperature values are set. When it is necessary to produce solar irradiance in cold conditions (>400 Wm^{-2} and <20 °C), the difference between the measured and programmed temperature can be over 5 °C. In those circumstances, a vertical temperature gradient of up to 2 °C directed upwards can be observed in the outdoor chamber. Furthermore, the values of the simulated solar irradiance are not entirely stable and fluctuate if the high level of radiation (>800 Wm^{-2}) is to be replicated in addition to relatively low outside air temperatures (<15 °C).

3. Methods for experimental assessment

This section presents an overview of the experimental methods that can be employed to investigate thermophysical phenomena in DSFs, given the flexibility of the designed testbed. To begin with, we provide details about the general verification of the experimental set-up and the reliability of airflow measurements, highlighting the importance of proper verification/calibration prior to experimental analyses, and show how reliable and coherent the measurements carried out with our testbed are. We also indicate the level of depth one can dive into when it comes to analyzing certain thermophysical phenomena. Thereafter, a basic characterization methodology is illustrated, referring to principles and guidelines accepted by the scientific community for measuring standardized metrics of ventilated and non-ventilated facade systems, such as solar heat gain coefficient, thermal and solar transmittance. However, to understand the behavior of DSFs under actual conditions that foresee the ventilation in the cavity, standardized measurements are not very helpful. Therefore, it is necessary to look for more detailed and non-standardized test methods. In this context, we present three alternative methods to study the comprehensive performance of DSF: 1) one-factor analysis, 2) design of the experiments (DOE), and 3) dynamic profile measurement. One-factor analysis implies analysis where the influence of a single factor is assessed by monitoring the dependent variable response to changes in only that factor. On the other side, the design of the experiment quantifies cause-and-effect relations between multiple factors and outputs in the studied system/process using statistical tools executed over results of systematically performed series of experiments [37]. The dynamic profile method aims to assess performance under 'real' transient conditions with the idea of simulating/-replicating 'typical days' where one can study the DSF.

3.1. Verification of the experimental set-up and uncertainty analysis

Although all sensors installed in the testbed were factory calibrated without further adjustments, coherence tests between measurements were performed from time to time to check the correctness of the data acquired through the system. For example, readings between different temperature sensors (three types, in total 60) were compared in thermal equilibrium when both chambers of the climate simulator had the same

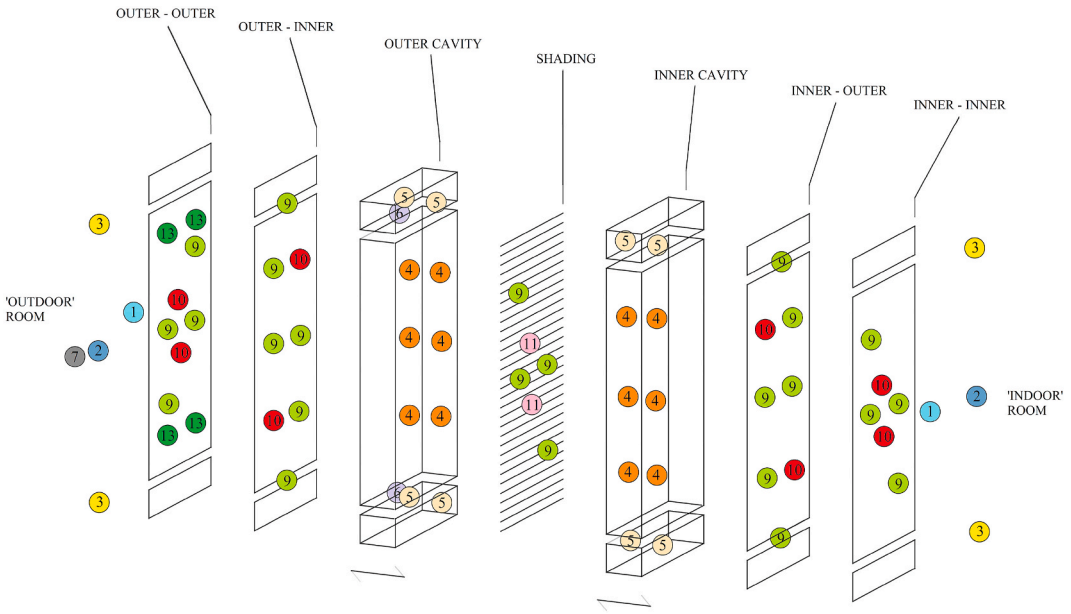

Fig. 3. Arrangement of sensors (for symbols, refer to Table 1).

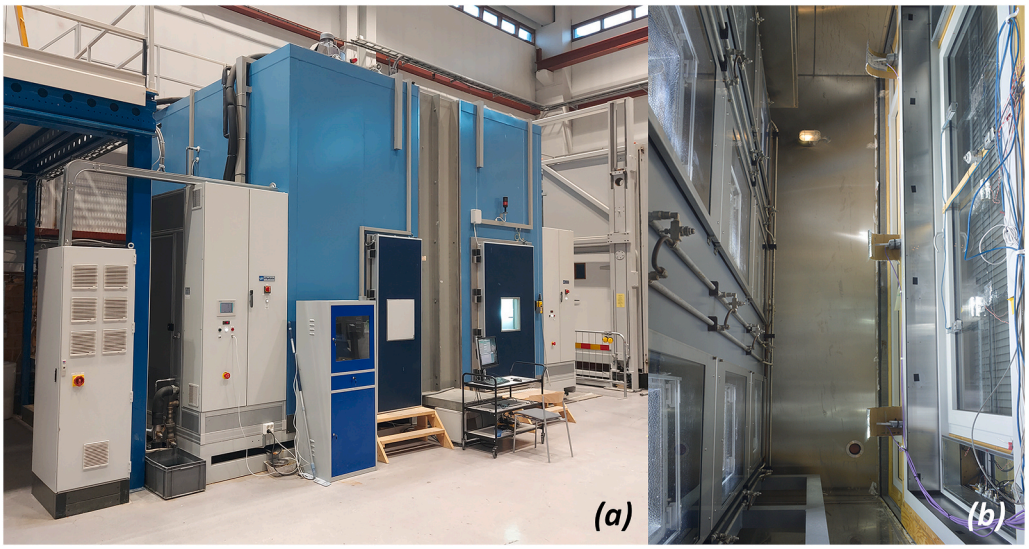

Fig. 4. The climate simulator facility (a); the DSF test sample placed in the climate simulator (b) - view from the outdoor chamber with the solar simulator's lamp array on the left-hand side of the picture and the DSF mock-up on the right-hand side of the picture).

temperatures. The sensors whose deviations with respect to the measurements of other sensors were larger than the instrument uncertainty were replaced, or their readings were calibrated [38]. The experimental uncertainty was then assessed using the method of error propagation [39], where the uncertainty of the final value is affected by the error of each sensor/device whose readings were used to calculate that value [40].

Monitoring the fluid dynamics behavior of double-skin facades represents the most delicate part of the thermal performance assessment [41]. The complexity is reflected through the sensitivity and accuracy of experimental equipment, which by their physical presence represent perturbation in the momentum field and thus influence the measurements. In addition to this, a short path to evolve a fully developed flow and variability in driving forces make measurements even more complicated. Since most techniques are either too complex to set up, such as particle image velocimetry (PIV) [42], or have an issue evaluating variable or low airflow rates, such as pressure difference or gas tracer method [43], there is no standardized method for measuring air flow rate in DSFs. Therefore, we opted for hot-wire anemometers and the velocity profile method (VPM) to estimate the airflow rates [44] as a trade-off between the complexity of the set-up, accuracy, desired amount of information and compatibility with the climate simulator facility that is combined with the flexible mock-up.

In order to determine the range of airflow rates in which this method can be considered reliable, it was necessary to verify the experimental set-up by comparing the reading through the VPM with one technique that could measure the bulk airflow rate so that punctual readings of velocity values and velocity profiles could be referenced to bulk airflow values. To perform this verification, a rectangular-to-round connector element was installed at the outlet so that the air leaving the cavity was collected and forced by means of a fan external to the cavity, an ultrasonic flow meter (Lindab UltraLink® Monitor) placed between the cavity and the fan. The ultrasonic flow meter (UFM) was capable of measuring low airflow rates with an uncertainty of $\pm 2\ ls^{-1}$ (or $7.2\ m^3h^{-1}$) for the given set-up. The controllable fan can force, given the set-up, an airflow in the range of 100 and 1000 m^3h^{-1}.

Values of velocity of the airflow in the cavity were recorded at three heights (¼, ½ and ¾ of DSF height), using four anemometers at each height. Velocity readings from two hot-wire anemometers installed at the first height were too discordant from the other values collected at ½ and ¾ of DSF height, so we omitted the corresponding velocity profile from the analysis as the robustness of this profile was not sufficient. At each height, two anemometers were installed close to glazing surfaces facing the cavity, the other two were placed one at each side of the shading device. The airflow rate was calculated based on the area of the velocity profile multiplied by the width of DSF, where the direction of the airflow (+ or – sign of velocity) was evaluated based on the temperature comparison with bordering surfaces. The comparison of measured airflows was made for two different cavity depths (40 and 60 cm) and several fan power consumptions (10, 15, 20, 25, 38, 63, 75, 88, and 100% of maximum power usage).

3.2. Measurement of standardized metrics

The climate simulator allows evaluation of the U-value using the methodology defined by the international standard ISO 9869-1 [45]. In order to determine the thermal transmittance, the heat flow meter (HFM) method was used, where the test element is exposed to steady-state conditions and the corresponding value is calculated using the simple average technique. The DSF was tested in the air-buffer ventilation mode and subjected to the temperatures of 0 °C in the 'outdoor' room and 20 °C in the 'indoor' room with no incident radiation. Simultaneously, the heat flux density was measured in two points on the inner side of the inner glazing. The average value of those two was considered representative for the calculation of the U-value of the glazed part of the DSF.

The assessment of the solar heat gain coefficient (SHGC, total solar energy transmittance, solar factor, g-value) of a full-scale test element is not standardized [36]. However, a total solar energy transmittance given by the ISO standard 9050:2003 [46] can be divided into solar transmittance and secondary heat transfer towards the inside by convection and longwave radiation [47]. Therefore, it is possible to measure it in the climate simulator by measuring an incident and transmitted solar radiation by pyranometers and the heat flux density that passes through the heat flux meter towards the interior. In this way, a small share of a heat flow that originates due to the temperature difference between inside and outside is assigned to the solar heat gains, but if the corresponding temperature difference is low, then this share is negligible. Measurement conditions were taken from the ISO standard 15099: 2003 [48], the environmental summer conditions set for a test apparatus that includes a solar simulator, climatic chamber and a metering box [49]: internal temperature of 25 °C, external temperature of 30 °C and incident solar radiation of 500 Wm^{-2}. Just like for the U-value measurements, the DSF test sample was set into the air-buffer ventilation

model, while the g-value was monitored for different cavity depths and angles of venetian blinds.

Moreover, thermal conductance of both glazing and heat transfer coefficients referent for the inner and outer surfaces (SHTC) were calculated from the referent measurements of heat flux density and air temperature. We calculated the measurement uncertainty of standardized metric, which consists of two parts; the uncertainty originating from the instrument limitations [45,50,51] and the standard deviation around the mean. As with most laboratory measurements in steady-state conditions, the part of the error emerging from the instrument imprecision is dominant over the statistical part. The uncertainty propagation method was used to assess the measurement error of indirectly measured quantity [39,40].

3.3. One-factor analysis

An experimental testbed allows a well-established method to investigate the impact of one parameter on one or more output variables by varying only that factor [52]. This strategy is also known as the one-factor analysis or local sensitivity analysis. It is a traditional approach to experimental investigation, where one can obtain detailed insight into how a change in a particular parameter affects other variables and the system's behavior. However, this approach can be misleading in examining the overall impact of a specific parameter in complex systems whose non-linear behavior is driven by the interaction of several factors [53]. There are different possibilities to carry out a one-factor analysis, depending on the goal of the investigation and the nature of the variables involved in the process. In this paper, we present, as an example, how the change of the airflow path affects temperature and velocity distribution in the cavity of a chosen DSF configuration during typical conditions:

- tropical summer day ($t_{out} = 40$ °C, $I = 800$ Wm^{-2}), DSF configuration (d = 60 cm, shading closed, 0°)
- tropical summer night ($t_{out} = 30$ °C, $I = 0$ Wm^{-2}), DSF configuration (d = 60 cm, shading open, 90°)
- mid-latitude warm winter day ($t_{out} = 10$ °C, $I = 400$ Wm^{-2}), DSF configuration (d = 60 cm, shading 45°)

Alternative versions of the one-factor analysis could have been to fix the airflow path and the boundary conditions, and gradually change one of the variables in the problems within the entire range of values (for example, the cavity depth or the opening size), or to change the value within a given (small) range around different baseline values. One of the challenges to bear in mind when employing this method to test small variations is that the resulting effect may be too small to be quantified with a suitable accuracy by the monitoring system. However, a change in a value too low to be detected can also be read as an important result – i.e., the independent variable has little impact on the dependent variable.

3.4. Design of experiments (DOE)

The DOE implies the application of statistical tools to quantify and classify relations between different variables and performance indicators in the studied process [37]. However, to obtain a good evaluation, a series of experiments need to be performed systematically. One of the efficient approaches can be factorial experimental arrays (designs). Here, the experiments are performed in a series where several factors are altered in each run, which enables the assessment of their impacts. If the array is well designed, the impact of interactions between factors can be assessed as well [54]. In the experimental campaign that lasted over several months, we tested several factorial designs and other arrays directly derived from factorial analysis to find an optimal design that will provide us with a comprehensive picture of the thermal and fluid dynamics behavior of DSFs. These arrays include full factorial, definitive screening, central composite (response surface) and multilevel Taguchi designs. In this paper, the intention is to present preliminary results of the experimental campaign and demonstrate the application of the DOE approach in the characterization of thermophysical behavior and performance of DSFs.

The array used here is the Taguchi 4Lx4F L16 array consisting of only 16 experimental runs where four different factors are discretized in four levels. Several response quantities that outline thermal and fluid dynamics behavior of DSF were chosen: airflow rate, net heat flux density associated with the DSF, heat gain/loss rate by the airflow that passes through the cavity normalized by the surface of DSF, the average temperature of the cavity and the average temperature of the inner surface of inner glazing (mathematical description is given in Table 2). The heat gain/loss rate through the convective heat exchange of the airflow becomes part of the net heat flux density for the indoor air ventilation mode since the airflow transfers heat, in that case, between the indoor environment and the cavity. The same quantity is not part of the net heat transfer in the outdoor ventilation mode, as in that case, airflow diverts heat towards the outside. Since it uses a relatively low number of experimental runs for such a high number of factors and levels, this design only offers insight into the main effects. However, it is good enough for an initial investigation into the processes that occur in DSF. Two different ventilation modes were tested separately via this array: indoor and outdoor air curtains.

3.5. Dynamic profile measurements

Besides measurements in the steady-state conditions, the climate simulator offers execution of the experiment in a dynamical environment where the temperature of both rooms, incident solar radiation and relative humidity can be preprogrammed. That allows insight into the thermal performance of DSFs during typical periods (summer or winter days) by examining dynamic diurnal profiles of specific quantities. Unlike natural experiments in a real outdoor environment [13,55,56], dynamic profile measurements in a controlled environment allow the researcher to focus on the specific situation, component of the façade system or driver of the performance, or to repeat the test to better capture the behavior of the system. On the other hand, these tests are usually limited because the wind effect cannot be replicated or because the climate simulator has its limitations, especially when it comes to the incident radiation adjustment. In our case, each lamp could be controlled only in the range between 50 and 100% of the maximum power, so we could not simulate the gradual increase and decrease of the incident solar radiation in the sunrise and sunset hours. Additionally, at

Table 2
Description of factors and response quantities.

Factors	Symbol	Unit	Levels			
			I	II	III	IV
Incident solar radiation	I	[Wm^{-2}]	0	400	600	800
Temperature difference	Δt	[°C]	−15	−5	5	15
Angle of venetian blinds	φ	[°]	OFF	0	45	90
Cavity depth	d	[cm]	20	30	40	60
Response quantities		***Unit***	***Equation***			
Net heat flux density associated with DSF	q_{net}	[Wm^{-2}]	$q_{HFM} + q_{tr} + (q_{vent})$			
The average temperature of the cavity	t_{cav}	[°C]	$\frac{\sum_{i=1}^{n} t_{cav,i}}{n}$			
Airflow rate	$\dot{V}$	[m^{3}h^{-1}]	Velocity profile method			
Heat gain/loss rate by the airflow that passes through the cavity normalized by the DSF surface	q_{vent}	[Wm^{-2}]	$\frac{\dot{m} c_p (t_{out} - t_{inl})}{A}$			
The average temperature of the inner surface of inner glazing	t_{ii}	[°C]	$\frac{\sum_{i=1}^{n} t_{ii,i}}{n}$			

high radiation levels, the irradiated energy is less stable than for other levels, probably due to the high-power consumption of the climate simulator.

The chosen DSF configuration was subjected to dynamic testing, corresponding to a typically hot summer day with high irradiation levels and outdoor temperatures. The temperature oscillated as a sine wave with the crest of 35 °C and trough of 20 °C, while incident solar radiation peaked around 770 Wm^{-2} with the previously referred lack of gradual rise/fall in simulated periods of sunrise (04:51) and sunset (19:45) (Fig. 5). The tested DSF had a 20 cm wide cavity with an outdoor air curtain airflow path, where the inlet was fully opened (42 dm^2) and the outlet less opened (7 dm^2). The shading system was placed in the middle position between the two skins of the DSF with partially opened slats (45°). The only buoyant-driven flow was examined without activation of the fans.

4. Results

4.1. Verification of the experimental set-up and uncertainty analysis

In total, 48 measurements were performed using two different methods for various DSF configurations, for which the results of comparisons are given in Fig. 6. For low airflow rates, the velocity profile method tended to overestimate airflow rate, most likely due to the velocities in the cavity below the instrumental threshold. Overall, there were no significant differences between airflow rates assessed by the velocity profile method on the ½ and ¾ height of the DSF, except for very high airflow rates where the cavity depth was 60 cm. For these configurations, the airflow at half of the cavity height tended to be higher than at three-quarters of the cavity, most likely due to sensors in the inner half-cavity that were in the path of a stronger air flow.

The accuracy of the VPM in evaluating the airflow rate was assessed through comparison with measurements of the ultrasonic flow meter. The relative error was taken as the indicator quantity of the reliability with a value of ±30% as an acceptable deviation. The airflow rate was divided by the cavity cross-section area to eliminate dependence on its size. The normalized quantity can be seen as the average velocity in the cavity since the airflow was unidirectional (upward). The distribution of relative error with normalized airflow rate is shown in Fig. 7. We can conclude that the velocity profile method was relatively accurate in the range of the normalized airflow rate between 360 and 1500 mh^{-1} (0.1–0.417 ms^{-1}), and most likely the upper threshold is even higher. However, due to the capacity of the duct fan, we were not able to assess it for higher airflow rates. Therefore, only the bottom threshold for the reliability of the velocity profile method is stated. For the cavity depth of 20 cm, the lower limit was around 100 m^3h^{-1}, 40 cm, 200 m^3h^{-1}, and 60 cm, 300 m^3h^{-1}. However, in natural DSFs, attention should be paid to the threshold value of air velocity rather than air flow rate. Lower airflow rates can be reliably assessed for bidirectional flows if the absolute value of measured air velocity is greater than 0.1 ms^{-1}.

4.2. Standardized metrics: U- and g-value

Values of thermal transmittance and solar factor were assessed for various configurations, including different cavity depths and angles of venetian blinds. Theoretical (expected) values fit well within the range of combined instrumental and measurement uncertainty (Table 3). There was a noticeable downward trend in thermal transmittance values with increasing cavity depth, as expected. Experimentally obtained values of the solar heat gain coefficient corresponded to the expected theoretical. Yet, it must be pointed out that measurement uncertainty was high, especially for the very low values of the solar factor, Table 3).

The high uncertainty is a consequence of the class of pyranometer (second) used for steady-state measurement of incident solar radiation, whereupon the main part of error originates from the uncertainty associated with the signal processing. Additionally, the assessment of the solar factor and direct solar transmittance was affected by the optical losses in the cavity, which become more pronounced as the cavity expands. As the cavity expands, the area of the lateral sides also increases, which means a larger surface that absorbs solar radiation. Therefore, a higher share of radiation is absorbed and lost for transmission, and consequently, the g-value is lower. Keeping all this in mind and compared with the test apparatus and procedure given with the standard ISO 19467, the assessment of g-value using HFM and pyranometer in a climate simulator can be considered approximate.

Indicated SHTC values characterize heat transfer during measurements of thermal transmittance, and they show weak fluctuations with DSF configuration change, which indicates the good stability of the measurement conditions. The climate simulator does not provide the ability to control the surface heat transfer coefficients (SHTC) at the borders of the test element and indoor/outdoor environments. However, similar values between them were observed, and their resemblance

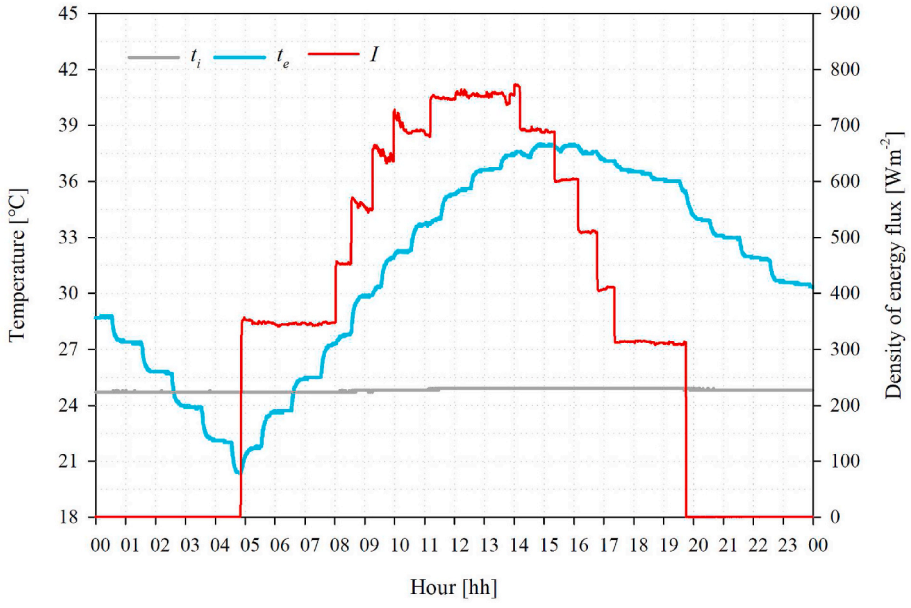

Fig. 5. Boundary conditions corresponding to a typical summer day.

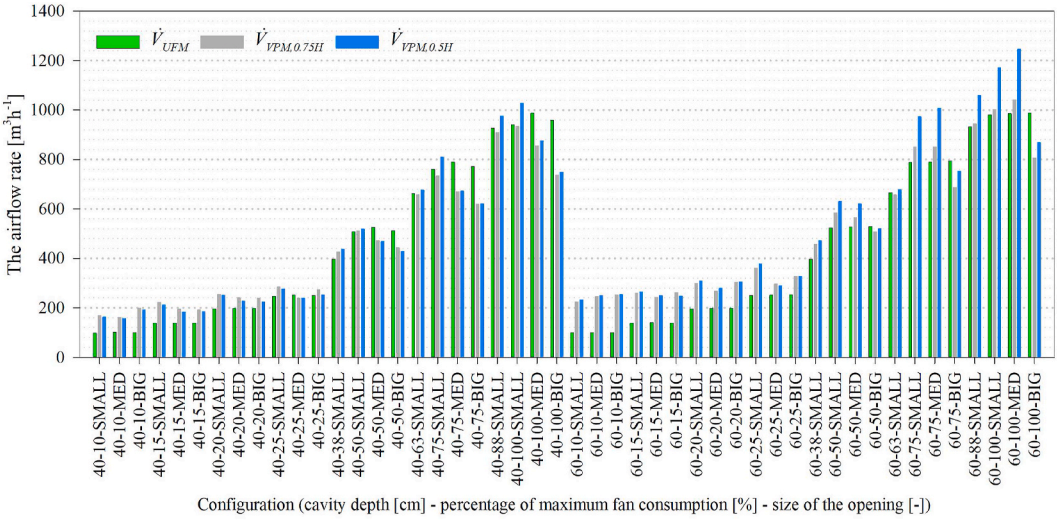

Fig. 6. The airflow measurement using ultrasonic flowmeter and velocity profile method at two different heights for different configurations of DSF.

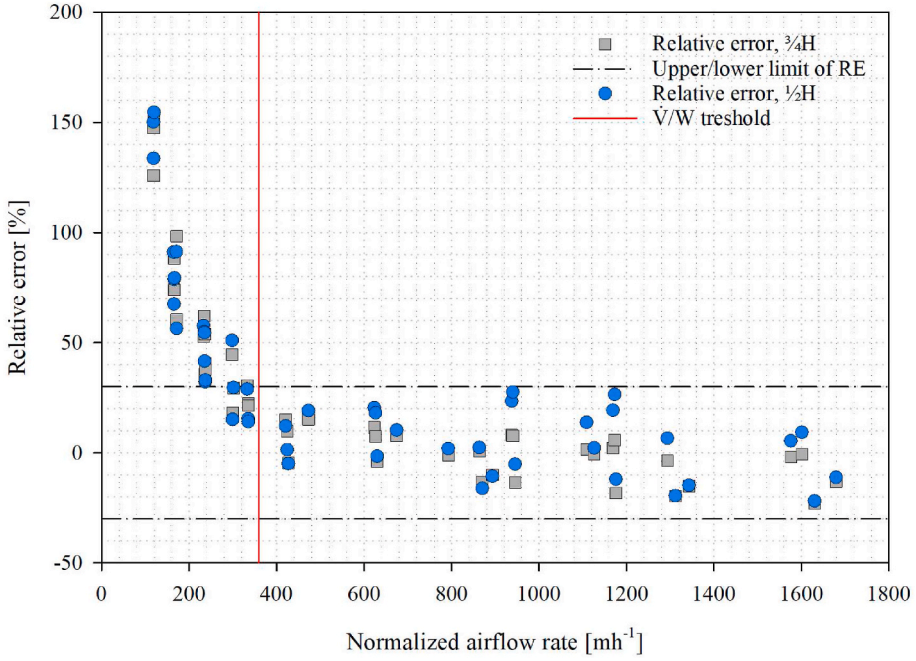

Fig. 7. Distribution of relative error with a normalized airflow rate.

originates from the similar conditions in both rooms regarding convective (mainly natural) and radiative heat transfer. SHTC at the cavity interfaces showed asymmetry and weaker heat transport on the outer side of the cavity. Although both double gazing units were made of the same materials and filled with the same gas mixture (air and argon in ratio 1:9), the measured value of thermal conductance differed by a non-negligible amount. The disparity may have originated due to the different thermophysical properties (density, dynamic viscosity, and thermal conductivity) of gas mixture caused by exposure to different temperatures [58]. However, we cannot claim this with certainty since the uncertainty range around the mean values of these two quantities overlaps.

4.3. One factor analysis

To showcase investigations that can be classified as one-factor analysis, we provide three examples of tests where the impact of only one variable is analyzed, which is, in this case, the path of the ventilation air that crosses the DSF. The results of the investigations show the strong impact that the ventilation mode had when the conditions are those of a *hot summer day*. Shifting from outdoor to indoor air curtain mode lowered the temperature of the cavity by about 15–20 °C (Fig. 8a). At the same time, the net heat transfer increased more than ten times (from 30 to 385 Wm^{-2}). Furthermore, shifting from O–O to I–I ventilation mode increased the airflow rate almost three times and stabilized upward motion in the inner half-cavity (Fig. 8b, $\dot{V}/W \sim$ from 260 $m^3m^{-1}h^{-1}$ to 810 $m^3m^{-1}h^{-1}$).

An example of not so relevant impact of a single factor is a change in the ventilation mode in *hot summer night* conditions. The temperature profile in the cavity remained flat, but it decreased by around 5 °C when changing from the O–O to the I–I ventilation mode, while the amount of heat entering the indoor environment remained quite low in both cases (Fig. 9a). The impact on the air dynamics was somewhat higher, as the

Table 3
Standard metrics measurement results (U-value, g-value, solar transmittance and heat transfer coefficients along with corresponding measurement uncertainties).

Configuration			*U-value*	*U-value error*	*g-value*	*g-value error*	τ_e	*Heat transfer coefficient*								*Conductance*			
Depth	*Shading*	*Angle*						h_{ii}	*err* h_{ii}	h_{ic}	*err* h_{ic}	h_{oc}	*err* h_{oc}	h_{oo}	*err* h_{oo}	C_{og}	*err* C_{og}	C_{ig}	*err* C_{ig}
mm	-	*0*	$Wm^{-2}K^{-1}$	$Wm^{-2}K^{-1}$	-		-	$[Wm^{-2}K^{-1}]$											
200	OFF	–	0.618	0.0572	0.346	0.0750	0.294	12.0	3.82	9.4	3.27	3.1	1.48	11.5	3.74	1.65	0.58	1.39	0.52
200	ON	0	0.617	0.0569	0.071	0.0125	0.020	12.3	3.89	8.8	2.82	2.7	1.22	11.7	3.86	1.79	0.63	1.47	0.54
200	ON	45	0.623	0.0563	0.138	0.0268	0.081	12.3	3.91	8.7	2.91	2.9	1.26	11.8	3.82	1.75	0.61	1.44	0.54
200	ON	90	0.623	0.0561	0.267	0.0563	0.215	12.3	3.89	8.9	2.97	2.9	1.28	11.9	3.86	1.75	0.62	1.45	0.54
400	OFF	–	0.608	0.0575	0.358	0.0731	0.281	11.7	3.67	9.6	3.09	2.8	1.24	12.4	4.03	1.63	0.57	1.40	0.51
400	ON	0	0.611	0.0570	0.059	0.0115	0.005	12.1	3.79	9.0	2.69	2.5	1.10	12.5	4.16	1.78	0.62	1.48	0.54
400	ON	45	0.616	0.0578	0.105	0.0202	0.059	12.1	3.77	8.9	2.91	2.6	1.14	12.4	4.07	1.76	0.62	1.44	0.53
400	ON	90	0.619	0.0559	0.223	0.0467	0.174	12.2	3.78	9.3	2.85	2.6	1.12	12.8	4.18	1.76	0.62	1.44	0.53
600	OFF	–	0.610	0.0571	0.265	0.0565	0.223	12.1	3.76	8.7	3.01	2.8	1.34	12.3	3.89	1.63	0.57	1.41	0.52
600	ON	0	0.593	0.0584	0.042	0.0114	0.007	12.6	3.89	8.1	2.71	2.4	1.15	12.0	3.86	1.64	0.57	1.42	0.52
600	ON	45	0.617	0.0575	0.085	0.0158	0.041	12.4	3.78	8.5	2.82	2.6	1.25	12.4	4.00	1.73	0.60	1.46	0.54
600	ON	90	0.611	0.0568	0.166	0.0340	0.123	12.1	3.81	9.0	2.86	2.6	1.24	12.5	3.99	1.71	0.60	1.45	0.54

airflow rate in both cases was net downward but was around eight times higher in outdoor air curtain mode (Fig. 9b, O–O: $\dot{V}/W \sim -390$ $m^3m^{-1}h^{-1}$, I–I: $\dot{V}/W \sim -50$ $m^3m^{-1}h^{-1}$). However, when it comes to the airflows assessed by the VPM, one should always check air velocity values and temperature differences between fluid and bordering surfaces to confirm the supposed direction of the airflow. For the same reason, we cannot claim the exact values and direction of particular streams in the flow in the given case.

As the last example of one-factor analysis, we analyzed the impact of ventilation mode in steady-state conditions corresponding to *a mid-latitude warm winter day*. One can notice that shifting from the outdoor to indoor air curtain mode increased temperatures in the cavity from around 10 to 13 °C (Fig. 10a), while the net heat flux density remained almost the same (O–O: $q_{net} = 36.0$ Wm^{-2}, I–I: $q_{net} = 31.4$ Wm^{-2}). In both ventilation modes, the outer half-cavity was slightly warmer than the inner due to multiple reflections and absorptions on the adjacent surfaces. Both ventilation modes were characterized by the strong upward current in the inner half-cavity with a circulatory motion in the outer half-cavity, only differing in its direction (Fig. 10b). From the given experimental data, one can envision how the naturally driven airflow is vital for removing excessive heat in the cavity ventilated by the outdoor air curtain. For the given case, a large amount of heat ($q_{vent} = 166$ Wm^{-2}) accumulated in the cavity was redirected to the outside by the airflow.

4.4. Design of experiments (Taguchi 4Lx4F L16 design, array with 16 experimental runs)

Results of the ANOVA analysis for the Taguchi design with 16 points (experimental runs) are given in Table 4 and shown in Fig. 11. Generally, analysis shows which factors drove the thermophysical behavior of DSF, and in the case of DSF with indoor air curtain ventilation mode, it was primarily the incident solar radiation. Here, we must emphasize again that this refers only to the intensity of solar radiation with directionality features proper of the solar simulator (where a certain quota of the irradiance fell in a range of angles close to 90° and another quota was due to reflected radiation that is likely to behave as the diffuse quota of solar radiation) since we could not control the direction of emitted radiation. Furthermore, one can notice that temperature difference played the second most important role in controlling heat gain/loss by the airflow, while for the temperature of the inner side of inner glazing, it was the angle of VB.

The thermal behavior of DSF with the outdoor air curtain ventilation mode is more diverse in comparison to the previous one, with temperature difference becoming dominant over solar radiation in controlling it. The temperature difference was the major factor in driving all response quantities, except net heat transfer, where solar radiation and the degree of openness of venetian blinds were dominant. The ANOVA can also indicate the structural element(s) most capable of manipulating the system performance. In the shown example, the shading device as a structural element had a large impact on the thermophysical behavior of DSF, and this influence was way greater than the cavity depth. However, there were some exceptions, such as the airflow in indoor air curtain ventilation mode, but here the conclusions related to cause-and-the-effect behavior of the airflow should be taken with caution due to the uncertainty of both the method and the sensors (check section 4.1).

4.5. Dynamic profile analysis of a typical hot summer day

As the last example of investigation type, we present the analysis of temporal profiles of quantities measured during dynamical boundary conditions that were designed to represent a typical hot summer day. The time profiles of the average temperature of the cavity (t_{cav}), shading device (t_{sh}), glazing surfaces (inner-inner t_{ii}, inner-outer t_{io}, outer-inner t_{oi}, and outer-outer t_{oo}), temperature gain/loss of the airflow in the cavity (Δt) and the airflow rate in the cavity ($\dot{V}$) are shown in Fig. 12. In

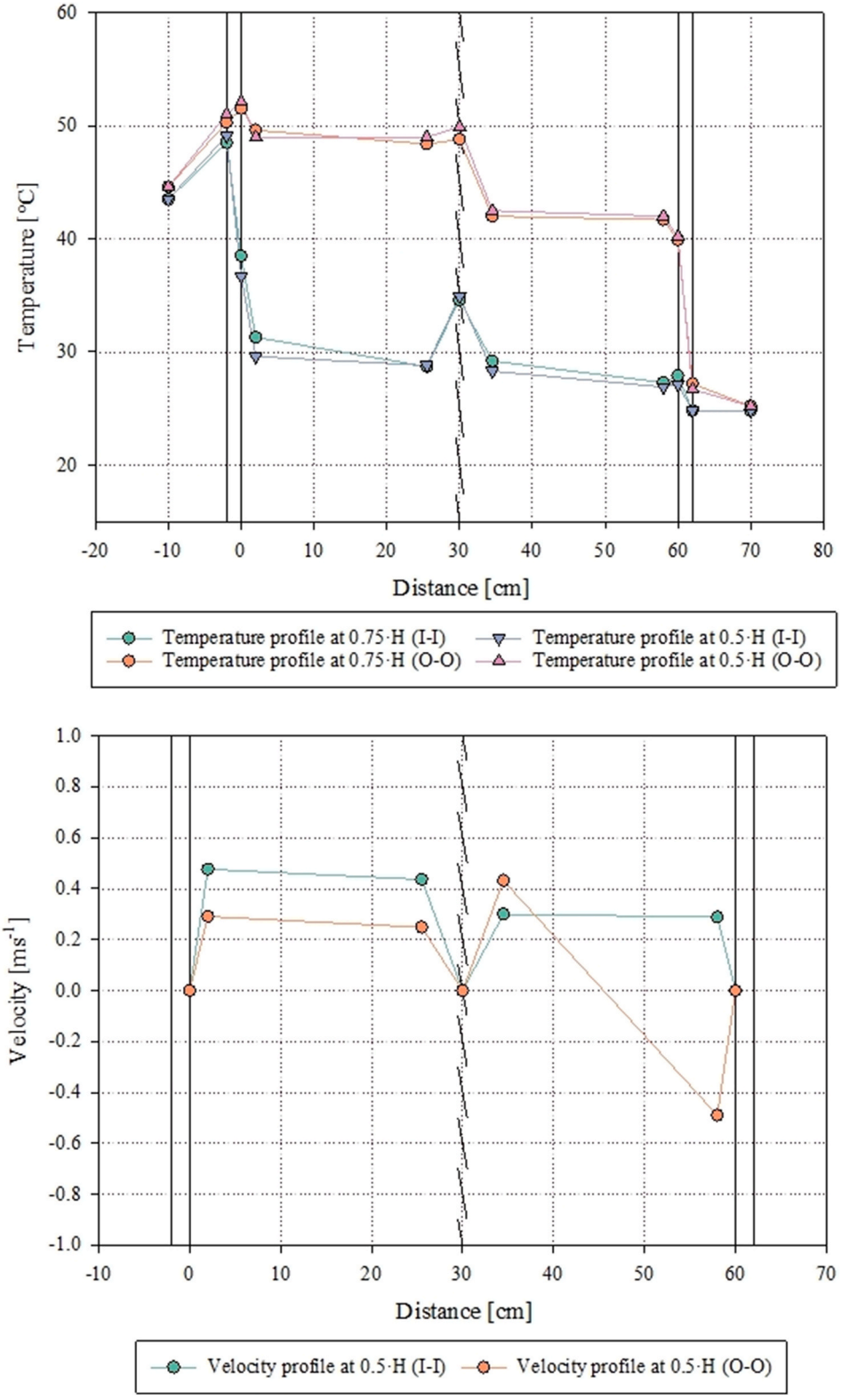

Fig. 8. a) Temperature and b) velocity profiles during a tropical summer day.

the provided example, it is noticeable that the temperature gain of the airflow passing through the cavity was higher than 5 °C in the central period of the day (between 10:00 and 15:30), while before the sunset and during most of the evening, there was no increase since the temperatures of the cavity borders became almost equal to the air temperature in the cavity.

One may draw important conclusions from the obtained profiles, such as for the airflow rate profile: around sunset, the airflow was unstable and oscillated between the upward and downward directions; during the daytime (between 06 and 18:30), the airflow stabilized its direction and rate with an average value around 125 m^3h^{-1} due to significantly hotter cavity borders; during the period without impinging

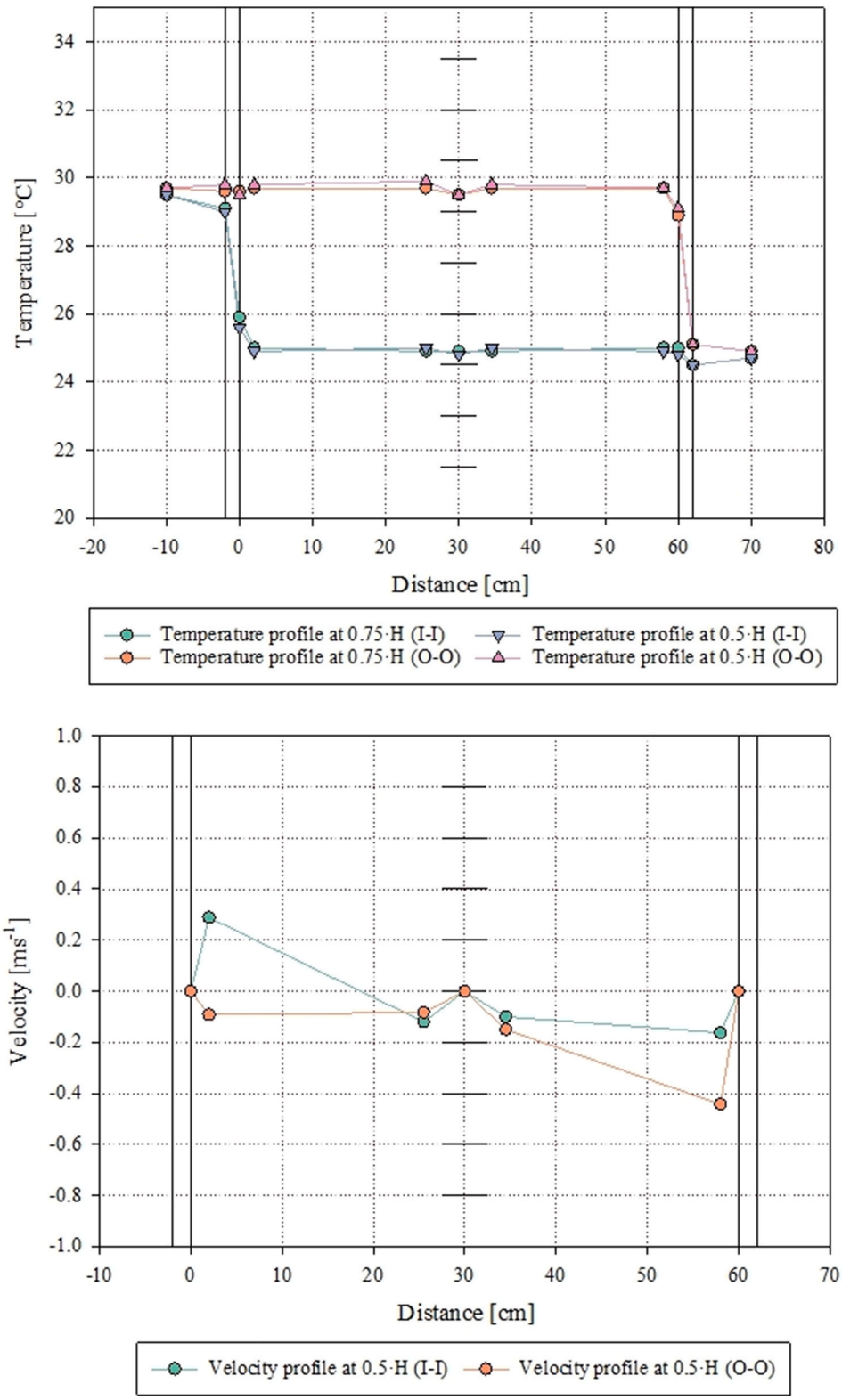

Fig. 9. a) Temperature and b) velocity profiles during a tropical summer night.

solar radiation (nighttime between 20 and 02), airflow shifted its direction downward with a relatively stable rate of about −125 to −150 m^3h^{-1}.

In the presented example from Fig. 13, one can notice how naturally induced airflow was a very useful mechanism for removing excess heat in the cavity ventilated with the outdoor air curtain mode (O–O). For example, in the period of intense solar radiation (between 10 and 15 h), almost 40% of the heat that reached the interior was directed to the outside (see Fig. 13, dynamic insulation efficiency is around 0.4) thanks to the airflow in the cavity. As defined in the work of Corgnati et al. [17], the dynamic insulation efficiency represents the quota of the heat flux

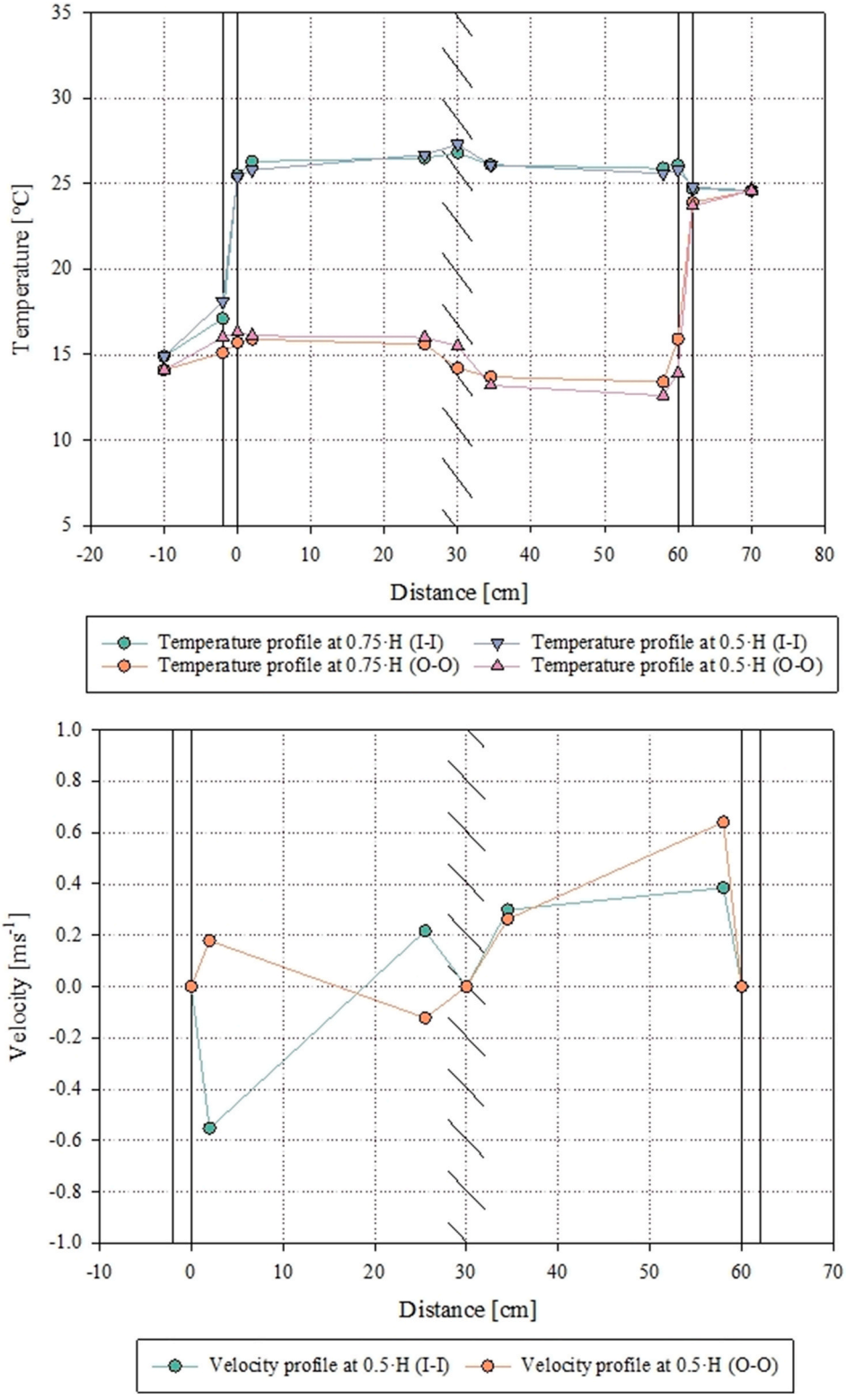

Fig. 10. a) Temperature and b) velocity profiles during a mid-latitude warm winter day.

Table 4
Contribution and statistical significance of factors (***p < 0.05***) in controlling indicators of thermal performance and dynamic behavior of fluid in the cavity obtained using a Taguchi design with 16 experiments followed by ANOVA.

Indoor air curtain	q_{net}		t_{cav}		$\dot{V}$		q_{vent}		t_{ii}	
	co [%]	p [−]	co [%]	p [−]	co [%]	p [−]	co [%]	p [−]	co [%]	p [−]
Solar irradiance	88.0	***0.004***	84.6	***0.003***	64.9	***0.003***	58.8	***0.007***	53.0	***0.033***
Temperature difference	8.2	0.1	7.0	0.088	10.5	***0.046***	28.3	***0.02***	3.2	0.580
Angle of VB	1.2	0.571	3.4	0.199	4.6	0.127	9.9	0.082	32.8	0.062
Cavity depth	1.1	0.612	3.9	0.176	19.0	***0.02***	1.4	0.526	6.8	0.347
Error	1.5	–	1.2	–	1.1	–	1.6	–	4.2	–
Outdoor air curtain	q_{net}		t_{cav}		$\dot{V}$		q_{vent}		t_{ii}	
	co [%]	***p [−]***	***co [%]***	***p [−]***	***co [%]***	***p [−]***	***co [%]***	***p [−]***	***co [%]***	***p [−]***
Solar irradiance	51.4	***0.05***	5.5	***0.002***	39.1	***0.006***	26.1	0.059	29.2	***0.030***
Temperature difference	1.4	0.85	94.3	***0.000***	45.4	***0.005***	60.6.	***0.019***	60.4	***0.011***
Angle of VB	34.2	0.084	0.1	0.498	11.9	***0.033***	5.1	0.352	5.9	0.211
Cavity depth	7.5	0.404	0.1	0.470	2.7	0.209	5	0.363	2.3	0.474
Error	5.5	–	0.1	–	0.9	–	3.2	–	2.1	–

that enters through the outer surface of the facade (and which would enter the room in the case of a traditional glazed facade) that is removed by the ventilation air. The calculation of the dynamic insulation efficiency[1] revealed a high-frequency noise originating from the airflow rate measurement. In order to eliminate this noise, the 10-min moving average was employed as a low-pass filter. From the extracted profile, one may find that in certain parts of the day, the airflow has no positive effect on the energy efficiency of DSF and that it increases net heat transfer (periods with zero value of dynamic insulation coefficient). That is evident during the hot nighttime period when the airflow is directed downward due to the colder bordering surfaces causing potentially negative (unrealistic) coefficient values. However, this effect is not so important for the considered typical day as the net heat flux density is not large in this part of the day.

Another example of an interesting finding in the dynamic profile analysis is the diurnal variation of the direct solar transmittance, shown in Fig. 14. The value of this quantity steadily grew towards the end of the period with imposed solar radiation (from 0.06 to 0.14). That occurred due to the lag between the profile of heat flux density measured by HFM and the profile of the transmitted solar radiation intensity (Fig. 14, compare maximums of q_{HFM} and I_{tr} profiles). One may notice that in the late part of the day (between 16 and 19), the heat flux density (measured by HFM) becomes equally significant as the transmitted solar radiation intensity. This effect has been seen in other experimental analyses in-field. Thus, obtaining similar results through this laboratory test shows that the developed testbed is capable of representing phenomena that are seen in systems implemented in real buildings, regardless of the limitations that the equipment presents (e.g., the limitation in replicating the full geometrical features of solar radiation).

The last example (Fig. 15) shows the profiles of airflow rate at two different heights and in two different segments of the cavity (inner and outer half-cavity). In order to smooth out high-frequency noise and increase the readability of the flow representation, a 2-min moving average was applied in the calculation of airflow rate profiles. The profiles indicate the complicated spatial structure of the flow that became even more delicate for the analysis due to its dynamical variability. However, from the shown profiles, some basic conclusions can be drawn. During the daytime, almost all mass flow occurred through the outer half-cavity, while during the nighttime, the situation reversed, and the flow became downward oriented and somewhat more intensive in the inner half-cavity. In the period before sunrise and around sunset, the flow became unstable and often changed its characteristics. The profiles can also indicate deficiencies of measurement methods, such as VPM. For example, the airflow rate on the 2nd height resembled the airflow rate measured at the 3rd height with a similar curve profile throughout the day, except in a few hours after sunset. The discrepancy probably results from the combined effects of several sources of uncertainty: imperfections of measurement method (point measurements in the space), instrument accuracy and the developing nature of the flow.

5. Lessons learned, possibilities and limitations

Transport processes in DSF are highly dynamic and in constant nonlinear interaction, making it very difficult to link the DSF constructive features with thermophysical behavior. The flexible testbed was developed and designed to operate in combination with the climate simulator to facilitate characterization and increase possibilities for systematic investigation of DSF systems. Several investigation approaches, including some non-standardized methods that provide a more detailed insight into thermal and fluid-dynamics system behavior, were tested. The whole campaign consisted of three equally important phases: the planning, the development of the experimental set-up and the execution of the experiment. Taught by the experience, we would like to discuss the issues we have encountered during this course, highlight the advantages of such an experimental approach and outline possibilities in future research.

In the planning phase, it is recommended to systematically design the sensor layout and data acquisition (DAQ) system, preferably through schematic and wiring diagrams, to facilitate the physical development of the set-up and the finding of the potential problems in communication with sensors. At this stage, it is essential to design an efficient strategy for conducting the experimental campaign, taking into account the desired depth of insight, available resources and limitations of the experimental set-up.

The sensor layout should be realized in this stage so that temperature sensors and heat flux meters are shielded from direct radiation. In some situations, space for ventilation needs to be provided to sensors to avoid excessive heat accumulated by the radiative absorption of the shield. Physical support, communication and power supply lines of sensors must be placed to affect thermal and velocity fields minimally. When it comes to an experimental set-up like this, where dozens of sensors and control features need to be used, it is compulsory to develop a system for automatic control and monitoring of the experiment. The DAQ system should consist of the controller or central processing unit connected to multiple transmitters, transducers and Modbus devices via a communication network systematically organized in sections of terminal blocks

[1] The dynamic insulation efficiency was obtained using the following equation: $\varepsilon = \frac{\dot{m}_v c_p (T_{exh} - T_i)}{\overline{q}_i A + q_s A + \dot{m}_v c_p (T_{exh} - T_i)}$ $\overline{q}_i$ - the average specific heat flux entering the indoor environment through the inner glass pane of the facade. q_s - the specific heat flux through the facade due to short wave radiation $\dot{m}_v$ – the mass flow rate that the air exhausted through the air gap of the facade T_{exh} and T_i, the inlet and outlet air temperature in the air gap, respectively.

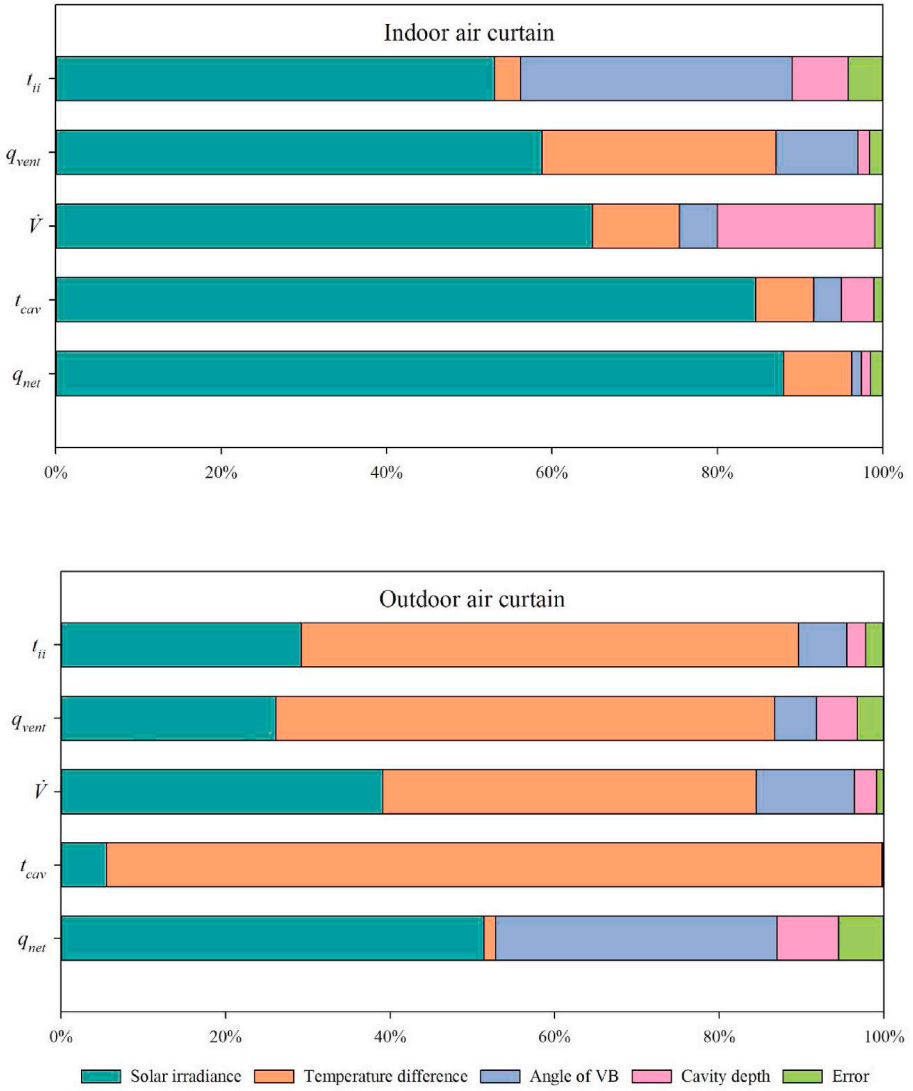

Fig. 11. Contribution of the factors to the variance of the response variables for two examined ventilation modes.

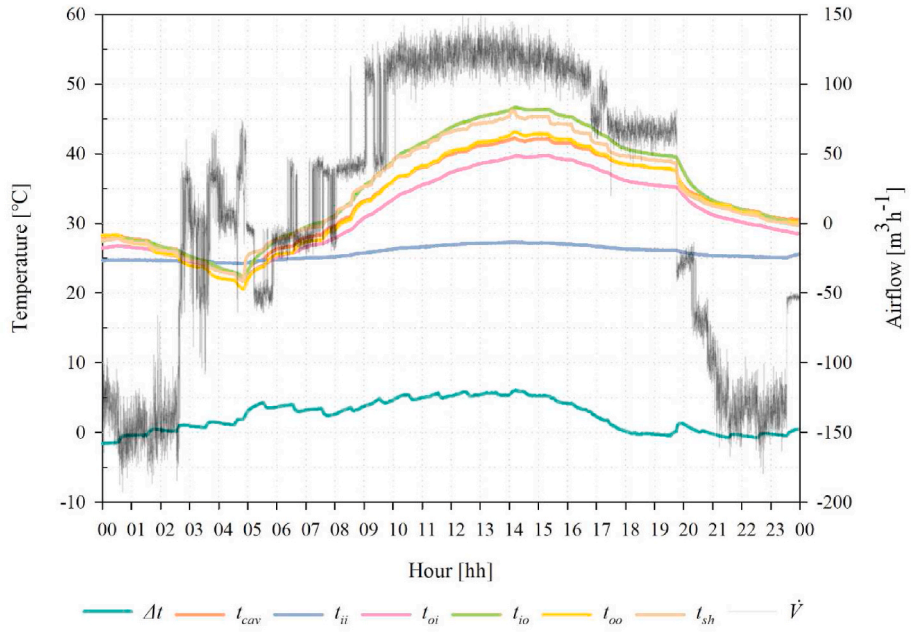

Fig. 12. Diurnal profiles of the average temperature of the cavity (t_{cav}), shading device (t_{sh}), glazing surfaces (inner-inner t_{ii}, inner-outer t_{io}, outer-inner t_{oi}, and outer-outer t_{oo}), temperature gain/loss of the airflow in the cavity (Δt) and the airflow rate in the cavity ($\dot{V}$).

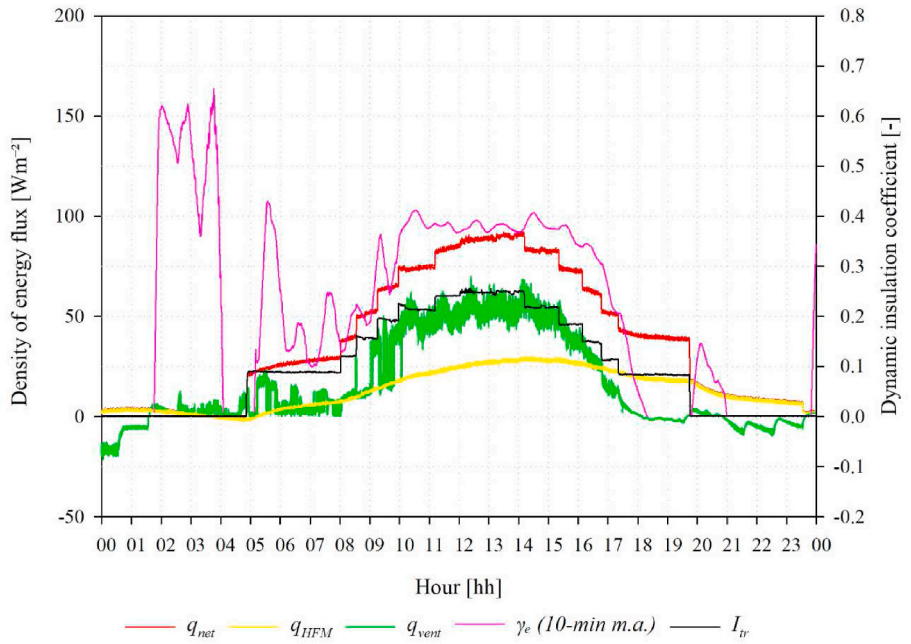

Fig. 13. Diurnal profiles of net heat flux density (q_{net}), the normalized heat rate gain/loss by the airflow (q_{vent}), heat flux density measured by HFM (q_{HFM}), transmitted solar radiation intensity (I_{tr}) and dynamic insulation efficiency (γ_e).

for easier communication handling.

Before the experimental campaign, it is necessary to check the reliability and validity of measurements and, if needed, to calibrate sensors. The temperature sensors should be checked by setting both chambers of the climate simulator in thermal equilibrium at known temperatures, preferably below, around and over the room temperature (e.g., 5, 20, and 35 °C), so one may inspect uniformity between measurements over various ranges. Coherence between measurements of energy flux meters (such as heat flux meters, pyranometers, or other types of radiometers) should be inspected by placing all sensors close together and inducing stimuli of different intensities. If the experimental campaign has a long duration (several months), it is necessary to perform the sensor checks several times during this period. Alternative measurement methods also need to pass accuracy checks and calibration to detect how comprehensive an analysis they can offer.

The standard metric measurements are a quite straightforward investigation type to perform as they require one to follow (where available) the standardized procedures. However, when determining optical properties (such as g-value or direct solar transmittance), some challenges can arise from the imperfections of the equipment and the test specimen. Though it is possible to obtain some values for standardized metrics for a DSF, most of the standard metrics cannot properly characterize the thermal and especially the fluid-dynamic behavior of DSFs as these technologies presents phenomena that are far from the

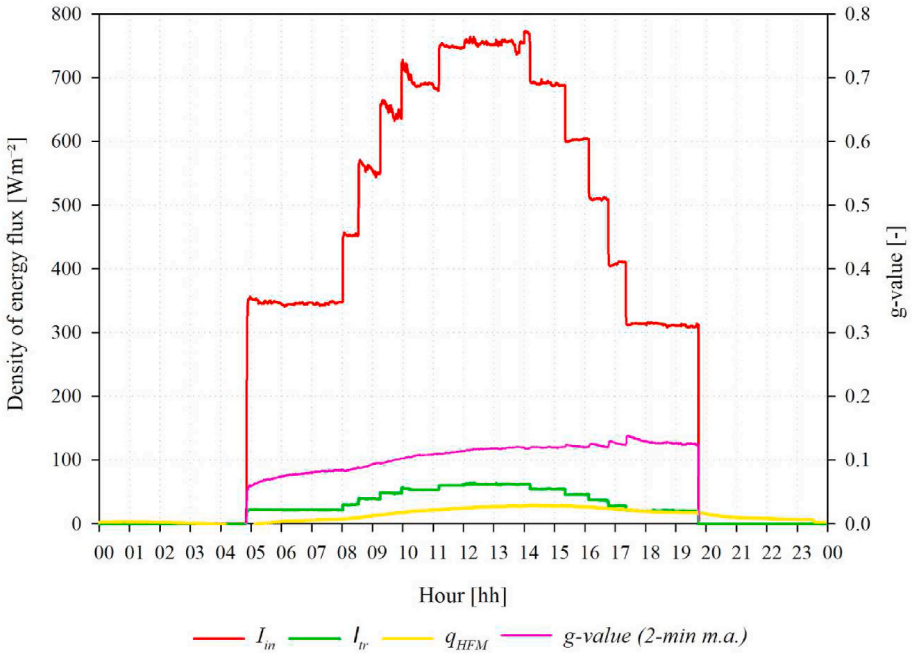

Fig. 14. Diurnal profiles of incident solar radiation intensity (I), transmitted solar radiation intensity (I_{tr}), heat flux density measured by HFM (q_{HFM}), and g-value (g).

assumptions behind the development of some standardized metrics (such as monotone temperature gradient or monodirectional heat flow). The one-factor analysis allows researchers to overcome the limitations set by standardized procedures and makes it possible to obtain some insight into the thermal and fluid-dynamic behavior of DSFs, though in a rather simplified way. This is because it is not possible to analyze and describe the simultaneous influence of several factors (interactions) on the variable of interest. The results of one-factor analyses can hardly be used to optimize or to predict DSF behavior fully, but they are most commonly used to analyze in depth a particular phenomenon or to obtain data for validation or calibration of numerical models. Sometimes, one-factor analyses are also used for pre-screening of important variables and key correlations between one independent variable and one dependent variable.

DOE is the most suitable way to balance accuracy, breadth and costs to obtain a complex system behavior characterization that includes the analysis of the impact of multiple factors and their interactions, including structural elements, operational modes and boundary conditions as independent variables. This investigation type requires a series of experiments in various steady-state conditions and therefore demands

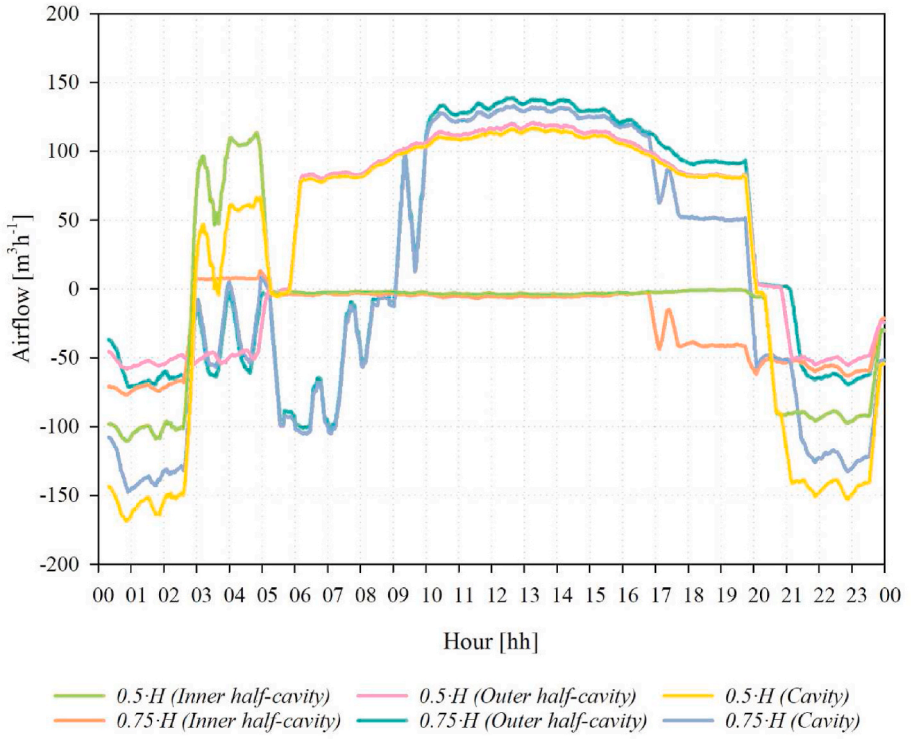

Fig. 15. Airflow rate measured in the inner and outer half-cavity at the 2nd and 3rd height.

substantial material costs. However, the expenses can be reduced with a few practical tips. For example, it is advisable to perform the DOE in two steps if it is necessary to examine the influence of many factors. The first one is to screen out important variables affecting the performance/behavior of the system, and the second is a more detailed analysis with a focus only on relevant factors. When it comes to DOE and its application to DSFs, we refer to our previous work for more information and the recommended course of action for performing DOE analysis, depending on the number of examined factors, the desired depth of insight and available resources [37]. Since the DOE approach requires the systematic execution of experiments, where several factors are altered during each experimental run, it is advisable to arrange the series so that factors are altered gradually between runs. The system will reach steady states faster by avoiding extreme alteration in factor values, such as the shift from bottom to peak values and vice versa. For example, priority should be given to a gradual change in ambient temperature. The system is thermally most inert to changes in chamber temperature, then in solar irradiance, and only after them in all other parameters, such as features of DSFs (e.g., blind angle, cavity depth, airflow path, or rate). Whether the system has reached a steady state can be checked conveniently and efficiently by inspection of air temperature readings in the cavity since this section of the DSF system adopts the latest stable values. In this way, an experimental campaign consisting of 15–20 runs can be shortened by several days. By applying the DOE, it is possible to describe the thermal and fluid-dynamical behavior in a wide range of conditions. This method can also be used to find optimal configurations and to build up (linearized) models that can predict the behavior of a DSF given certain boundary conditions and structural properties, even if the exact combination has not been experimentally tested.

The dynamic profile measurements imply experimental investigation in dynamic boundary conditions that usually correspond to the fluctuation of the boundary conditions in typical (design) days. Unlike the other investigation types, this method captures thermal and fluid dynamics behavior in conditions close to the real ones found when envelope systems are deployed in real buildings, and it is suitable for testing responsive façade systems. This analysis can lead to system optimization, but only in given conditions, and probably has its highest value in the joint analysis of the building technology and the control to manage its (dynamic) performance. In the case of dynamic profile measurements for a typical day, it is desirable to perform a series of measurements corresponding to several consecutive identical days to consider the effect over a longer period and to prevent initial conditions from playing a role in the results.

However, some limitations of the equipment and the applied measurement methods restrict the possibilities of thoroughly investigating the thermal and fluid dynamics behavior of DSF. For example, the climate simulator may simulate conditions that deviate from the desired one. For example, when it is necessary to maintain the low or intermediate temperature of the outdoor chamber (<25 °C) and at the same time to have an active solar simulator, the air conditioning system can experience problems in controlling the outdoor chamber temperature. The actual temperature is a few degrees higher than the set-point and the air is not uniformly cooled through the chamber, which results in a vertical temperature gradient up to 2 °C directed upwards. The reason for this is probably the combined effect of climate simulator overload and the inappropriate position of the integrated temperature sensor used to regulate the set-point temperature of the outdoor chamber.

Even though the solar simulator is calibrated to provide homogeneity of irradiance within reasonable limits (around ±10%), this property deteriorates over time due to physical changes in radiation surface, position and different aging of the lamps. Furthermore, in extreme settings where the high irradiance (>800 Wm^{-2}) is combined with low set-point temperature (<15 °C), the solar simulator experiences problems in maintaining time-stable irradiated power, which can fluctuate in range ±10% from the desired one. In addition to this, irradiance significantly attenuates with distance from radiation surface. The inability of the solar simulator to impose and control low radiation levels (below 250 Wm^{-2}) is a significant disadvantage that restricts reproducing particular conditions, such as low irradiance levels characteristic for a winter day or gradual increase or decrease of irradiance typical for sunrise/sunset periods. Moreover, as already pinpointed, the lamp array in the climate simulators does not offer the possibility of controlling the direction of emitted radiation. The inability to control the impinging angle represents a limitation of the solar simulator since the thermal performance (the solar reflectance and transmittance) of both the glazing and the shading device depends on the incident angle [59,60]. However, even if the system cannot allow one to obtain reliable results on the effect of the geometry of solar radiation on the performance of the system, much information can still be obtained on the role of the different layers in the construction and how they interact with the solar radiation.

When it comes to the disadvantages of the test sample, the limited width represents a notable issue that causes optical loss, which is particularly pronounced when the cavity is maximally expanded. Therefore, slightly lower values of the solar factor and direct solar transmittance are obtained compared to those expected. Setting a constant irradiance on the outer surface of the DSF for different cavity widths is not a straightforward task since the irradiance attenuates with retraction of the outer skin of the DSF. Therefore, constant checking and readjustment of the bulb's power is advised.

Regarding the measurement methods, the VPM has shown unreliability when it comes to evaluating the low airflow rates (average velocity below 0.1 ms^{-1}). Furthermore, determining the airflow direction and especially heat transfer coefficients using temperatures of fluid and the bordering surfaces is unreliable if the temperature difference is below the instrumental error (below 0.3 or 0.5 °C). Likewise, punctual measurements cannot accurately capture the velocity profile, especially in thick cavities where the boundary layer effect is considerable. Therefore, the naturally driven airflows that usually have a complex structure with bidirectional patterns could be inappropriate for the airflow rate characterization using VPM. Alternative techniques to measure airflow in such situations, such as laser Doppler (LDV), particle image (PIV) and ultrasound velocimetry, could be employed if the scope of the investigation requires. However, complexity, technical limitations and costs associated with these techniques could make it unfeasible in the context of these studies.

In an effort to make our research freely accessible and to allow maximum usability of the collected data, all the measurements presented in this study to demonstrate the functionalities of the test bed and the applications of the different experimental methods (cft. Section 4.1, 4.3 and 4.4) have been uploaded to on an open-access repository. Data can be found at, and referenced using, the following weblink: https://doi.org/10.5281/zenodo.5808012.

6. Conclusions

Thermophysical processes occurring in advanced building envelopes, such as DSF, are very intercorrelated and complicated to analyze. The experimental approach is the only way to reliable describe them, but it is rigid, time-consuming and expensive. To overcome these drawbacks and systematically study the thermal and fluid-dynamic behavior of DSFs, we have developed a flexible experimental testbed and validated its functioning with a series of experimental procedures. Different DSF configurations can be easily tested in response to various boundary conditions thanks to a purpose built DSF mock-up and a climate simulator that can recreate boundary conditions, including temperature gradient and solar irradiation. A developed system for data acquisition and control of the experiment enables the adjustment of desired DSF configuration and environmental conditions and simultaneous monitoring of more than seventy sensors in real-time.

In the description presented in the paper, we highlighted the features of the flexible experimental testbed, its sensitivity and reliability, and discussed different types of experimental investigations with various

levels of complexity: standard metrics measurements, one-factor analysis, design of experiments and dynamic profile measurements. In this manuscript, we have provided examples of each investigation type, showed the advantages and disadvantages of the different techniques, and discussed challenges and possibilities associated with them. The main take-home message that we want to convey is that complementary analyses are necessary, and depending on the scope of the investigations, one or more combinations of methods should be employed to obtain the desired knowledge of the specific performance or phenomenon. A comprehensive set of data from the measurements carried out to test and validate the testbeds and the methods has been made publicly available to the scientific community, and is especially targeted at researchers working with numerical model development, validation, and model calibration, who could benefit from the freely accessible dataset for comparison between experimental and numerical data.

By presenting some examples of different types of investigations, we have also given a preview of certain insights about the impact of structural elements, operational modes and boundary conditions on the thermal and fluid dynamics behavior of DSFs, though this was not the focus of the study. Some limitations of the testbed restrict the possibility of investigating all the possible phenomena in DSF. The impact of solar geometry and complete flow characterization are two examples of domains that cannot be fully addressed by the developed experimental equipment, though it allows obtaining some information. The preliminary findings previewed in this paper will be expanded in future studies that will focus on the specific relations between constructional features and performance in DSFs.

Though the testbed developed so far is suitable to investigate DSF systems, the same approach involving a flexible mock-up and the development of optimized experimental procedure can be applied to any advanced building envelope system to obtain a comprehensive picture of the behavior of these complex systems in the most efficient way.

CRediT authorship contribution statement

Aleksandar Jankovic: Writing – original draft, Methodology, Investigation, Formal analysis, Data curation, Conceptualization. **M. Salman Siddiqui:** Writing – review & editing, Supervision, Methodology, Investigation, Data curation. **Francesco Goia:** Writing – review & editing, Supervision, Resources, Project administration, Methodology, Funding acquisition, Formal analysis, Conceptualization.

Declaration of competing interest

The authors declare that they have no known competing financial interests or personal relationships that could have appeared to influence the work reported in this paper.

Acknowledgements

The activities presented in this paper were carried out within the research project “REsponsive, INtegrated, VENTilated - REINVENT – windows”, supported by the Research Council of Norway through the research grant 262198, and the partners SINTEF, Hydro Extruded Solutions, Politecnico di Torino and Aalto University. The authors would like to thank Odne Oksavik from SINTEF Community for his support in developing the software for control and data acquisition. The technical partner Hydro Extruded Solutions (Hydro Building Systems) is also gratefully acknowledged for its support in developing and engineering the flexible mock-up and the in-kind contribution for its construction.

References

[1] E. Oesterle, R.-D. Lieb, M. Lutz, W. Heusler, Double-skin Facades : Integrated Planning, München : Prestel, 2001.
[2] R.A. Agathokleous, S.A. Kalogirou, Double skin facades (DSF) and building integrated photovoltaics (BIPV): a review of configurations and heat transfer characteristics, Renew. Energy 89 (2016) 743–756.
[3] M.S. Siddiqui, A. Jankovic, F. Goia, Design and testing of a flexible test bed for thermal and fluid mechanic investigations of double skin façades, in: Conference Proceedings of 15th RoomVent 2020 Conference, 2021.
[4] A. Jankovic, F. Goia, D. Eckert, P. Müller, A test bed for thermal fluid dynamic analysis of double skin facade systems, IOP Conf. Ser. Mater. Sci. Eng. 609 (2019) 32006.
[5] A. Jankovic, F. Goia, Impact of double skin facade constructional features on heat transfer and fluid dynamic behaviour, Build. Environ. 196 (2021), 107796, https://doi.org/10.1016/j.buildenv.2021.107796.
[6] A. Zöllner, E.R.F. Winter, R. Viskanta, Experimental studies of combined heat transfer in turbulent mixed convection fluid flows in double-skin-façades, Int. J. Heat Mass Tran. 45 (22) (2002) 4401–4408.
[7] D. Saelens. Energy performance assessment of single storey multiple-skin facades, Catholic University of Leuven, 2011.
[8] L.C.O. Souza, H.A. Souza, E.F. Rodrigues, Experimental and numerical analysis of a naturally ventilated double-skin façade, Energy Build. 165 (2018) 328–339.
[9] F. Yang, F. Yuan, F. Qian, Z. Zhuang, J. Yao, Summertime thermal and energy performance of a double-skin green facade: a case study in Shanghai, Sustain. Cities Soc. 39 (2018) 43–51.
[10] G. Michaux, R. Greffet, P. Salagnac, J.B. Ridoret, Modelling of an airflow window and numerical investigation of its thermal performances by comparison to conventional double and triple-glazed windows, Appl. Energy 242 (2019) 27–45.
[11] Y. Luo, L. Zhang, Z. Liu, L. Xie, X. Wang, J. Wu, Experimental study and performance evaluation of a PV-blind embedded double skin façade in winter season, Energy 165 (2018) 326–342.
[12] C. Zhang, W. Gang, J. Wang, X. Xu, Q. Du, Numerical and experimental study on the thermal performance improvement of a triple glazed window by utilizing low-grade exhaust air, Energy 167 (2019) 1132–1143.
[13] J. Curpek, M. Cekon, J. Hraska, PCM integrated in BiPV ventilated façade concepts: experimental test cell platform and initial full-scale measurements, IOP Conf. Ser. Earth Environ. Sci. 290 (2019) 12072.
[14] S. Preet, M.K. Sharma, J. Mathur, A. Chowdhury, S. Mathur, Performance evaluation of photovoltaic double-skin facade with forced ventilation in the composite climate, J. Build. Eng. 32 (2020) 101733.
[15] H. Choi, Y. An, K. Kang, S. Yoon, T. Kim, Cooling energy performance and thermal characteristics of a naturally ventilated slim double-skin window, Appl. Therm. Eng. 160 (2019) 114113.
[16] H. Manz, A. Schaelin, H. Simmler, Airflow patterns and thermal behavior of mechanically ventilated glass double facades, Build. Environ. 39 (9) (2004) 1023–1033.
[17] S.P. Corgnati, M. Perino, V. Serra, Experimental assessment of the performance of an active transparent façade during actual operating conditions, Sol. Energy 81 (8) (2007) 993–1013.
[18] O. Kalyanova, P. Heiselberg. Experimental Set-up and Full-scale Measurements in the ‘Cube’, Department of Civil Engineering, Aalborg University, Aalborg, 2008.
[19] Y. Li, J. Darkwa, G. Kokogiannakis, Heat transfer analysis of an integrated double skin façade and phase change material blind system, Build. Environ. 125 (2017) 111–121.
[20] Z. Zeng, X. Li, C. Li, Y. Zhu, Modeling ventilation in naturally ventilated double-skin façade with a Venetian blind, Build. Environ. 57 (2012) 1–6.
[21] D. Brandl, T. Mach, M. Grobbauer, C. Hochenauer, Analysis of ventilation effects and the thermal behaviour of multifunctional façade elements with 3D CFD models, Energy Build. 85 (2014) 305–320.
[22] X. Hong, M.K.H. Leung, W. He, Effective use of Venetian blind in Trombe wall for solar space conditioning control, Appl. Energy 250 (Sep. 2019) 452–460.
[23] B. Koo, K. Lee, Y. An, K. Lee, Solar heat gain reduction of ventilated double skin windows without a shading device, Sustainability 10 (2) (Dec. 2017) 64.
[24] K.J. King. Turbulent Natural Convection in Rectangular Air Cavities, Queen Mary University of London, 1989.
[25] Y. Katoh, M. Miyamoto, J. Kurima, S. Kaneyasu, Turbulent free convection heat transfer from vertical parallel plates : effect of entrance bell-mouth shape, in: JSME Int. journal. Ser. 2, Fluids Eng. heat Transf. power, Combust. Thermophys. Prop. 34, 1991, pp. 496–501, 4.
[26] M.M. Gibson, A.A. Dafa’Alla, Two-equation model for turbulent wall flow, AIAA J. 33 (8) (Aug. 1995) 1514–1518.
[27] C. Popa, D. Ospir, S. Fohanno, C. Chereches, Numerical simulation of dynamical aspects of natural convection flow in a double-skin façade, Energy Build. 50 (2012) 229–233.
[28] W. Ding, Y. Hasemi, T. Yamada, Natural ventilation performance of a double-skin façade with a solar chimney, Energy Build. 37 (4) (2005) 411–418.
[29] N. Kimouche, Z. Mahri, A. Abidi-Saad, C. Popa, G. Polidori, C. Maalouf, Effect of inclination angle of the adiabatic wall in asymmetrically heated channel on natural convection: application to double-skin façade design, J. Build. Eng. 12 (2017) 171–177.
[30] O.A. Tkachenko, et al., Numerical and experimental investigation of unsteady natural convection in a non-uniformly heated vertical open-ended channel, Int. J. Therm. Sci. 99 (2016) 9–25.
[31] Y. Cherif, E. Sassine, S. Lassue, L. Zalewski, Experimental and numerical natural convection in an asymmetrically heated double vertical facade, Int. J. Therm. Sci. 152 (2020) 106288.
[32] L. Mei, et al., The influence of blinds on temperatures and air flows within ventilated double-skin facades, in: Proc. Clima 2007, WellBeing Indoors, 2007.

[33] V. Gavan, M. Woloszyn, F. Kuznik, J.-J. Roux, Experimental study of a mechanically ventilated double-skin façade with Venetian sun-shading device: a full-scale investigation in controlled environment, Sol. Energy 84 (2) (2010) 183–195.
[34] T. Inan, T. Basaran, Experimental and numerical investigation of forced convection in a double skin façade by using nodal network approach for Istanbul, Sol. Energy 183 (2019) 441–452.
[35] "REsponsive, INtegrated, VENTilated - REINVENT - windows." Research project grant 262198 by The Research Council of Norway. Website: https://prosjektbanken.forskningsradet.no/project/FORISS/262198?Kilde=FORISS&distribution=Ar&chart=bar&calcType=funding&Sprak=no&sortBy=score&sortOrder=desc&resultCount=30&offset=0&Fritekst=reinvent.
[36] F. Goia, V. Serra, Analysis of a non-calorimetric method for assessment of in-situ thermal transmittance and solar factor of glazed systems, Sol. Energy 166 (2018) 458–471.
[37] A. Jankovic, G. Chaudhary, F. Goia, Designing the design of experiments (DOE) – an investigation on the influence of different factorial designs on the characterization of complex systems, Energy Build. 250 (2021) 111298.
[38] C.W. Hurley, J.F. Schooley, Calibration of temperature measurement systems installed in buildings, Build. Sci. 153 (1984).
[39] J.P. Holman, Experimental Methods for Engineers, McGraw-Hill/Connect Learn Succeed, New York, N.Y., 2012.
[40] T. Başaran, T. İnan, Experimental investigation of the pressure loss through a double skin facade by using perforated plates, Energy Build. 133 (2016) 628–639.
[41] E. Giancola, et al., Possibilities and challenges of different experimental techniques for airflow characterisation in the air cavities of façades, J. Facade Des. Eng. 6 (3) (Aug. 2018), https://doi.org/10.7480/jfde.2018.3.2470. Spec. Issue FAÇADE 2018 – Adapt.
[42] N. Safer, Modélisation des façades de type double-peau équipées de protections solaires : approches multi-échelles, L'Institut National des Sciences Appliquées de Lyon, 2006.
[43] A. Jankovic, G. Gennaro, G. Chaudhary, F. Goia, F. Favoino, Gas traces techniques for airflow characterization in double skin facades, in: RoomVent, 2020, p. 2021.
[44] O. Kalyanova, R.L. Jensen, P. Heiselberg, Measurement of air flow rate in a naturally ventilated double skin façade, in: Proceedings of Roomvent 2007: Helsinki, FINVAC ry, 2007, 13-15 June 2007.
[45] International Organization for Standardization. ISO 9869-1: 2014 Thermal Insulation, Building Elements, In-Situ Measurement of Thermal Resistance and Thermal Transmittance-Part 1: Heat Flow Meter Method, ISO, 2014.
[46] International Organization for Standardization, ISO 9050: 2003, Glass in Building—Determination of Light Transmittance, Solar Direct Transmittance, Total Solar Energy Transmittance, Ultraviolet Transmittance and Related Glazing Factors, 2003.
[47] B.P. Jelle, Solar radiation glazing factors for window panes, glass structures and electrochromic windows in buildings—measurement and calculation, Sol. Energy Mater. Sol. Cells 116 (2013) 291–323.
[48] International Organization for Standardization, ISO 15099: 2003 Thermal Performance of Windows, Doors and Shading Devices, 2003.
[49] International Organization for Standardization, ISO 19467:2017 Thermal Performance of Windows and Doors — Determination of Solar Heat Gain Coefficient Using Solar Simulator, 2017.
[50] International Organization for Standardization, ISO 9060:2018(en) Solar energy — Specification and classification of instruments for measuring hemispherical solar and direct solar radiation, 2018.
[51] J. Konings, A. Habte, Uncertainty Evaluation of Measurements with Pyranometers and Pyrheliometers, 2016.
[52] S.M. Zahraee, M. Hatami, N. Mohd Yusof, J. Mohd Rohani, F. Ziaei, Combined use of design of experiment and computer simulation for resources level determination in concrete pouring process, J. Teknol. 64 (1) (Nov. 2013).
[53] D.C. Montgomery, Design and Analysis of Experiments, John Wiley & Sons, New York, 2001.
[54] N.R. Smalheiser, in: N.R. Smalheiser (Ed.), Chapter 5 - Experimental Design: Design Strategies and Controls, Academic Press, 2017, pp. 65–85.
[55] J. Parra, A. Guardo, E. Egusquiza, P. Alavedra, Thermal performance of ventilated double skin façades with Venetian blinds, Energies 8 (6) (2015) 4882–4898.
[56] R. Fuliotto, F. Cambuli, N. Mandas, N. Bacchin, G. Manara, Q. Chen, Experimental and numerical analysis of heat transfer and airflow on an interactive building facade, Energy Build. 42 (1) (2010) 23–28.
[58] International Organization for Standardization, EN 673:1997 Glass in Building – Determination of Thermal Transmittance (U value) – Calculation Method, 1997.
[59] G. Kokogiannakis, J. Darkwa, C. Aloisio, Simulating thermochromic and heat mirror glazing systems in hot and cold climates, Energy Proc. 62 (2014) 22–31.
[60] G. Baldinelli, Double skin façades for warm climate regions: analysis of a solution with an integrated movable shading system, Build. Environ. 44 (6) (2009) 1107–1118.

Further reading

[61] A. Jankovic, M.S. Siddiqui, F. Goia, An experimental data set on the thermal and fluid dynamic performance of double skin facades (DSFs) subjected to various controlled boundary conditions through the use of a climate simulator facility, 2021, https://doi.org/10.5281/zenodo.5808012.